scientific reports

OPEN

Synthesis of pyrido-annelated [1,2,4,5]tetrazines, [1,2,4] triazepine, and [1,2,4,5] tetrazepines for anticancer, DFT, and molecular docking studies

Aisha Y. Hassan[1], Sara N. Shabaan[1], Samiha A. El-Sebaey[2] & Eman S. Abou-Amra[1]✉

In this strategy, we attempt to design various novel nitrogen-rich heterocycles in one molecule. Green, simple, and efficient aza-annulations of an active, versatile building block, 1-amino-4-methyl-2-oxo-6-phenyl-1,2-dihydropyridine-3-carbonitrile (1), with different bifunctional reagents were developed under solvent-free conditions, resulting in the bridgehead tetrazines and azepines (triazepine and tetrazepines). Pyrido[1,2,4,5]tetrazines have been synthesized through two pathways; [3 + 3]- and [5 + 1]-annulations. In addition, pyrido-azepines have been developed by applying [4 + 3]-and [5 + 2]-annulations. This protocol establishes an efficient technique for synthesizing essential biological derivatives of 1,2,4,5-tetrazines, 1,2,4-triazepines, and 1,2,4,5-tetrazepine, tolerating a diverse variety of functionalities without the need for catalysis and fast reaction rates in high yields. The National Cancer Institute (NCI, Bethesda, USA) examined twelve compounds produced at a single high dosage (10^{-5} M). Compounds 4, 8, and 9 were discovered to have potent anticancer action against certain cancer cell types. To explain NCI results, the density of states was calculated to conduct a better description of the FMOs. The molecular electrostatic potential maps were created to explain a molecule's chemical reactivity. In silico ADME experiments were performed to better understand their pharmacokinetic characteristics. Finally, the molecular docking investigations on Janus Kinase-2 (PDB ID: 4P7E) were carried out to study the binding mechanism, binding affinity, and non-bonding contacts.

Heterocyclic compounds containing the pyridine[1] nucleus show a wide range of interesting biological effects, such as anticancer[2–4], antioxidant[5,6], antimicrobial[2,6,7], and anti-viral[8]. Furthermore, it has been demonstrated that 1,2,4-triazepines have a wide spectrum of therapeutic and biological effects[9–11].

Moreover, 1,2,4,5-tetrazines are a family of heterocyclic compounds having a diverse variety of biological actions, including anticonvulsant, anti-inflammatory, and antibacterial properties[12]. Many studies have shown that several 1,2,4,5-tetrazine compounds exhibit anticancer activity[13–15].

Tetrazepines are seven-membered azaheterocyclic molecules with valuable medical and pesticide applications[16]. Tetrazepine derivatives interest chemists and pharmacists, but there are only a few ways to synthesize them. Because of the importance of tetrazepines in pharmaceuticals and their wide variety of uses[17], great emphasis has lately been dedicated to the synthesis of novel tetrazepines as well as new methodologies.

In light of the above findings, following the pot, atom, and step economy (PASE)[18] concept aims to reduce the number of steps required to synthesize various fused heterocyclic structures as the vessel must be operated economically in a single reaction vessel without any of the requirement for workup or transitional species separation. We provide a simple method for synthesizing several bioactive nitrogen heterocycles regarding the idea of 'solvent-free', including fused pyrido-1,2,4-triazepines, 1,2,4,5-tetrazines, and 1,2,4,5-tetrazepines.

Computational chemistry is a prominent method for investigating the biological characteristics of recently produced compounds. Density functional theory (DFT) is a quantitative quantum mechanical modelling

[1]Department of Chemistry, Organic Chemistry, Faculty of Science (Girls), Al-Azhar University, Youssef Abbas Street, Nasr City, Cairo, Egypt. [2]Department of Pharmaceutical Organic Chemistry, Faculty of Pharmacy (Girls), Al-Azhar University, Youssef Abbas Street, Nasr City, Cairo, Egypt. ✉email: emansadek.59@azhar.edu.eg; eman.sadek.1612@gmail.com

approach used to explore the thermal and electrical stability of the produced compounds in this work. This study's determined parameters include dipole moment, the highest occupied molecular orbital (HOMO), the lowest unoccupied molecular orbital (LUMO), and the subtraction (HOMO–LUMO) gap energies. The molecular electrostatic potential surfaces (MEPs) were computed using Gauss View to measure their chemical and thermal characteristics.

Molecular docking is a bioinformatics modelling technique that deals with the interaction of two or more molecules to produce a stable adduct. The primary goal of molecular docking is to anticipate the possible binding geometries of produced molecules with a target protein in a three-dimensional structure. As many small ligands with JAK2 inhibitory activity produced therapeutic effects, and visualization of the compounds' greatest binding mode into Janus Kinase-2 (PDB ID: 4P7E) than other proteins, using the computer software Molecular Operating Environment (MOE), the more active compounds were investigated in silico to highlight their likely binding energy and interaction patterns with the active site of JAK2 (PDB ID: **4P7E**). The more potent compounds were then screened for drug-likeness using Lipinski's rule of five and ADME characteristics.

Experimental

Chemistry. All melting points were measured and uncorrected in open glass capillaries using an Electrothermal LA 9000 SERIS digital melting point instrument. Bruker high-performance digital FT-NMR spectrometer Avance III was used to scan the ^{1}H,^{13}C NMR spectra at [(600, 400) & 213] MHz in deuterated dimethyl sulfoxide and chloroform (DMSO-d_6 & $CDCl_3$) as a solvent. Mass spectra were acquired at 70 eV using a Schimadzu GC/MS-QP-5050A mass spectrometer et al.-Azhar University's regional center for mycology and biotechnology.

General procedure for the synthesis of compounds (2, 3, 5–7). Equivalent amounts of **1**[19] (2.25 g, 10 mmol) and each of [cyanoguanidine (0.84 g, 10 mmol), chloroacetone (0.92 g, 10 mmol), anthranilic acid (1.37 g, 10 mmol), hydrazinecarbonitrile (0.58 mL, 10 mmol), or thiosemicarbazide (0.91 g, 10 mmol)] were fused at 150–170 °C for 3 h. The fused mass was allowed to cool, triturated with ethanol, and then the precipitate was filtered, washed with ethanol, and dried.

N-(8-Cyano-7-methyl-5-phenyl-[1,2,4]triazolo[1,5-a]pyridin-2-yl)cyanamide (2). Yellow crystals are obtained, crystalized from EtOH/DMF (40/60%); yield (79) %, mp.: 228–230 °C; FT-IR (KBr, ν, cm^{-1}): 3190(NH), 3003(CH-Ar), 2980 (CH-aliph.), 2230, 2150 (2(C≡N), 1608(C=N); ^{1}H NMR (400 MHz, DMSO-d_6) δ(ppm): 2.51 (s, 3H, CH_3), 3.80(br., 1H, NH–C≡N, exchangeable with D_2O), 7.29–7.56 (m, 5H, Ar–H), 8.09 (s, 1H, CH-pyridine). ^{13}C NMR (213 MHz, $CDCl_3$) δ(ppm): 29.24(CH_3),111.23 (pyridine C–C≡N), 118.93 (C≡N),125.11 (CH-pyridine), 128.87, 129.73, 138.00 (phenyl C), 146.18 (2C=N), 156.37 (pyridine C–CH_3), 170.61 (pyridine C–Ph). MS (m/z, %): 274.08 ($M^{+\cdot}$, 31); 272.08 ($M^{+\cdot}$–2H, 29); 141.84 (100). Anal. Calcd. for $C_{15}H_{10}N_6$ (274.29); C, 65.68; H, 3.67; N, 30.64. Found C, 65.75; H, 3.77; N, 30.76.

4-Methyl-2-oxo-1-((2-oxopropyl)amino)-6-phenyl-1,2-dihydropyridine-3-carbonitrile (3). Orange crystals are obtained, crystallized from EtOH; yield (85) %, mp.: 115–118 °C; FT-IR (KBr, ν, cm^{-1}): 3400 (OH tautomer), 3250(NH), 3000, 2890 (CH), 2220 (C≡N), 1650, 1630 (2C=O), 1590 (C=N); ^{1}H NMR: (400 MHz, DMSO-d_6) δ(ppm): 2.24, 2.29 (2s, 6H, CH_3 & CH_3-tautomer); 2.19 (2s, 6H, COCH_3 & COCH_3—tautomer); 3.80 (s, 2H, CH_2); 4.17, 4.28 (2s, 2H, NH & NH—tautomer, exchangeable with D_2O); 5.05(s, 1H, =CH(tautomer)); 6.50, 6.55 (2s, 2H, CH-pyridine & CH-tautomer); 7.30–7.73 (m, 10H, Ar–H), 10.51 (s, 1H, OH(tautomer), exchangeable with D_2O). MS (m/z, %): 281.46(M^+, 16); 138.67(100). Anal. Calcd. for $C_{16}H_{15}N_3O_2$ (281.32); C, 68.31; H, 5.37; N, 14.94. Found C, 68.39; H, 5.42; N, 15.05.

3,9-Dimethyl-2,7-diphenyl-2,5-dihydropyrido[1,2-b][1,2,4,5]tetrazepine-10-carbonitrile (4). Equivalent amounts of **3** (2.81 g, 10 mmol) and phenylhydrazine (1.08 mL, 10 mmol) were fused at 150–170 °C for 2.5 h. The resultant solid was triturated with ethanol, filtered, washed by ethanol, dried, and crystallized from EtOH.

Brown crystals are obtained; yield (72) %, mp.: 241–243 °C; FT-IR (KBr, ν, cm^{-1}): 3170 (NH), 3020 (CH-Ar), 2870 (CH-aliph.), 2150 (C≡N); 1600 (C=N); ^{1}H NMR (400 MHz, DMSO-d_6) δ(ppm): 2.22, 2.24 (2s, 6H, 2CH_3), 2.65(s, 1H, NH-tetrazepine, exchangeable with D_2O), 4.18 (s,1H, CH-tetrazepine), 7.25–7.58 (m, 10H, Ar–H), 7.73 (s, 1H, CH-pyridine). ^{13}C NMR (213 MHz, $CDCl_3$) δ (ppm): 15.62 (CH_3), 21.20 (CH_3), 95.07(CH-pyridine), 104.75 (CH-tetrazepine),118.81 (C≡N), 119.06, 119.24, 122.15, 122.37, 126.07, 126.25, 129.00, 130.15, 131.73 (phenyl C). MS (m/z, %): 353.66 ($M^{+\cdot}$, 9); 352.56($M^{+\cdot}$–H, 23); 328.22(100). Anal. Calcd. for $C_{22}H_{19}N_5$ (353.43); C, 74.77; H, 5.42; N, 19.82. Found, C, 74.80; H, 5.48; N, 19.78.

2-Methyl-7-oxo-4-phenyl-6,7-dihydrobenzo[e]pyrido[1,2-b][1,2,4]triazepine-1-carbonitrile (5). Brown powder are obtained, crystallized from EtOH; yield (78) %, mp.: 189–191 °C; FT-IR (KBr, ν, cm^{-1}): 3420 (NH/OH), 3005 (CH–Ar), 2890 (CH–aliph.), 2226 (C≡N), 1625 (C=O); 1605 (C=N); ^{1}H NMR: (400 MHz, $CDCl_3$) δ(ppm): 2.20 (s, 3H, CH_3), 7.17–7.85 (m, 9H, Ar–H), 7.40 (s, 1H, CH–pyridine), 10.24(s, 1H, NH, exchangeable with D2O). ^{13}C NMR (213 MHz, DMSO-d_6) δ (ppm): 24.31 (CH_3), 95.63 (CH–pyridine), 117.98 (C≡N), 122.03, 122.36, 124.75, 128.50, 128.68, 129.42, 138.62, 141.79, 143.40 (phenyl C), 148.17 (C=N), 162.56 (C=O). MS (m/z, %): 323.51($M^{+\cdot}$–3H, 9); 94.24 (100). Anal. Calcd. for $C_{20}H_{14}N_4O$ (326.36); calc. C, 73.61; H, 4.32; N, 17.17. Found C, 73.64; H, 4.30; N, 17.15.

3-Amino-8-methyl-6-phenyl-4H-pyrido[1,2-b][1,2,4,5]tetrazine-9-carbonitrile (6). VYellow crystals are obtained, crystallized from EtOH; yield (67) %, mp.: 187–189 °C; FT-IR (KBr, ν, cm^{-1}): 3380, 3250, 3120 (NH_2, NH), 3010 (CH–Ar), 2950 (CH–aliph.), 2227 (C≡N), 1611 (C=N). Anal. Calcd. for $C_{14}H_{12}N_6$ (264.29); C, 63.62; H, 4.58; N, 31.80. Found C, 63.72; H, 4.52; N, 31.73.

3-Amino-8-methyl-6-phenyl-2H-pyrido[1,2-b][1,2,4,5]tetrazine-9-carbonitrile (7). Yellow crystals are obtained, crystallized from EtOH; yield (89) %, mp.: 202–204 °C; FT-IR (KBr, ν, cm^{-1}): 3300, 3220 (NH_2, NH), 3000 (CH-Ar), 2900 (CH-aliph.), 2170 (C≡N), 1610 (C=N). ^{1}H NMR (400 MHz, DMSO-d_6) δ (ppm): 2.25 (s, 6H, CH_3, CH_3(tautomer)), 6.43(s, 2H, NH_2, exchangeable with D_2O), 7.25–7.40 (m, 5H, Ar–H), 7.73, 7.75 (2 s, 2H, CH-pyridine & CH-pyridine (tautomer)), 8.07 (s, 1H, NH-tetrazine (tautomer), exchangeable with D_2O), 12.38, 12.60 (2s, 2H, =NH, NH-tetrazine, exchangeable with D_2O). ^{13}C NMR (213 MHz, DMSO-d_6) δ(ppm): 15.34, 15.63 (CH_3, CH_3 (tautomer)), 89.35, 94.23 (CH–pyridine, CH–pyridine (tautomer)), 117.36 (C≡N), 120.68, 121.49, 125.36, 129.28, 139.00, 140.40 (phenyl C). MS (m/z, %): 264.80 ($M^{+\cdot}$, 9); 262.47 ($M^{+\cdot}$–2H, 25); 50.27 (100). Anal. Calcd. for $C_{14}H_{12}N_6$ (264.29); C, 63.62; H, 4.58; N, 31.80. Found C, 63.72; H, 4.52; N, 31.89.

General procedure for the synthesis of compounds (8–10). Equivalent amounts of **7** (2.64 g, 10 mmol) and each of [(diethylmalonate (1.58 g, 10 mmol), phenacyl bromide (1.97 g, 10 mmol) or diethyl oxalate (1.47 mL, 10 mmol)] were fused at 150–180 °C for 3 h. The produced mass was allowed to cool, triturated with ethanol, and then the precipitate was filtered, washed with ethanol, dried, and crystallized from EtOH.

8-Methyl-2,4-dioxo-10-phenyl-1,2,3,4-tetrahydropyrido[1,2-b]pyrimido[1,2-e][1,2,4,5]tetrazine-7-carbonitrile (8). Orange crystals are obtained; yield (78) %, mp.: 250–252 °C; FT-IR (KBr, ν, cm^{-1}): 3420 (OH tautomer), 3380 (NH), 3000 (CH-Ar), 2970(CH-aliph.), 2225 (C≡N), 1750, 1670 (2C=O), 1600 (C=N). ^{1}H NMR (400 MHz, DMSO-d_6) δ(ppm): 2.14 (s, 3H, CH_3), 3.38 (s, 2H, CH_2-pyrimidindione), 7.16–7.45 (m, 5H, Ar–H), 8.05, 8.07 (2s, 2H, CH-pyridine & CH-pyridine (tautomer), 8.33, 8.36 (2s, 2H, NH-pyrimidindione & NH-pyrimidindione (tautomer), exchangeable with D_2O), 12.08, 12.09 (br.,2H,2OH(tautomer), exchangeable with D_2O). ^{13}C NMR (213 MHz, DMSO-d_6) δ (ppm): 17.13 (CH_3), 43.47 (CH_2), 88.05 (CH-pyridine), 118.42(C≡N), 121.01, 124.89, 125.45, 129.34, 138.59, 139.41 (phenyl C), 160.74, 163.55 (2C=O). MS (m/z, %): 332.05 ($M^{+\cdot}$, 25); 309.49(100). Anal. Calcd. for $C_{17}H_{12}N_6O2$ (332.32); C, 61.44; H, 3.64; N, 25.29. Found, C, 61.35; H, 3.52; N, 25.21.

7-Methyl-2,9-diphenyl-3H-imidazo[1,2-b]pyrido[1,2-e][1,2,4,5]tetrazine-6-carbonitrile (9). Orange crystals are obtained; yield (85) %, mp.: 258–260 °C; FT-IR (KBr, ν, cm^{-1}): 3100 (CH-Ar), 2970 (CH-aliph.), 2215 (C≡N), 1609(C=N). ^{1}H NMR (400 MHz, DMSO-d_6) δ(ppm): 2.08 (s, 3H, CH_3), 4.59 (s, 2H, CH_2-imidazole), 7.28–7.76 (m, 10H, Ar–H), 7.40 (s,1H, CH-pyridine). ^{13}C NMR (213 MHz, $CDCl_3$) δ(ppm): 22.94(CH_3), 52.29 (CH_2-imidazole), 99.54 (CH-pyridine), 119.40 (C≡N), 120.82, 121.15, 125.88, 126.60, 128.84, 129.41, 137.42, 138.37 (phenyl C). MS (m/z, %): 364.39 ($M^{+\cdot}$, 28); 198.96 (100). Anal. Calcd. for $C_{22}H_{16}N_6$ (364.41); C, 72.51; H, 4.43; N, 23.06. Found C, 72.45; H, 4.49; N, 23.02.

7-Methyl-2,3-dioxo-9-phenyl-2,3-dihydro-1H-imidazo[1,2-b]pyrido[1,2-e][1, 2, 4, 5] tetrazine-6-carbonitrile (10). Orange crystals are obtained; yield (74) %, mp.: 143–145 °C; FT-IR (KBr, ν, cm^{-1}): 3300 (NH), 3000 (CH-Ar), 2870 (CH-aliph.), 2220 (C≡N), 1750, 1650 (2C=O), 1600(C=N). ^{1}H NMR (400 MHz, DMSO-d_6) δ (ppm): 2.25 (s, 3H, CH_3), 7.25–7.73 (m, 5H, Ar–H), 7.75 (s, 1H, CH-pyridine), 8.63 (s, 1H, NH-imidazole, exchangeable with D_2O). ^{13}C NMR (213 MHz, DMSO-d_6) δ (ppm): 20.81 (CH_3), 87.75 (CH-pyridine), 116.70 (C≡N), 121.36, 125.12, 129.33, 137.56, 138.40 (phenyl C), 175.17, 175.70 (2C = O). MS (m/z, %): 318.44 ($M^{+\cdot}$, 23); 248.85 (100). Anal. Calcd. for $C_{16}H_{10}N_6O_2$ (318.30); C, 60.38; H, 3.17; N, 26.40. Found C, 60.46; H, 3.25; N, 26.49.

1-Amino-2-hydrazono-4-methyl-6-phenyl-1,2-dihydropyridine-3-carbonitrile (11). Equivalent amounts of **1**[19] (2.25 g, 10 mmol) and hydrazine hydrate (0.4 mL, 10 mmol) were fused at 120–140 °C for 3 h. The reaction mixture was allowed to cool, triturated with ethanol, and then the precipitate was filtered, washed with ethanol, dried, and crystallized from EtOH.

Orange powder are obtained; yield (84) %, mp.: 176–178 °C; FT-IR (KBr, ν, cm^{-1}): 3352, 3315(NH_2), 3003 (CH-Ar), 2990 (CH-aliph.), 2250 (C≡N), 1608 (C=N). ^{1}H NMR (600 MHz, DMSO-d_6) δ (ppm): 2.11 (s, 3H, CH_3), 4.50(s,2H, NH_2, exchangeable with D_2O), 5.49 (s, 2H, =N–NH_2, exchangeable with D_2O), 7.28 (s, 1H, CH-pyridine), 6.99–7.29 (m, 5H, Ar–H). ^{13}C NMR (213 MHz, DMSO-d_6) δ (ppm): 19.01(CH_3), 90.34(CH-pyridine), 118.11(CN), 120.44, 123.72, 125.07, 130.07, 134.61 (phenyl C), 146.49 (C=N). MS (m/z, %): 239.72($M^{+\cdot}$, 18); 71.42(100). Anal. Calcd. for $C_{13}H_{13}N_5$ (239.12); C, 65.25; H, 5.48; N, 29.27. Found C, 65.20; H, 5.53; N, 29.34.

General procedure for the synthesis of compounds (12–16). Equivalent amounts of **11** (2.39 g, 10 mmol) and each of [phenylisothiocyanate (1.35 mL, 10 mmol), chloroacetone (0.92 mL, 10 mmol), phenacyl bromide (1.97 g, 10 mmol), diethyl oxalate (1.47 mL, 10 mmol) or 3,4-dimethoxybenzaldehyde (1.66 g, 10 mmol)] were fused at 140–160 °C for 2 h. The fused mass was allowed to cool, triturated with ethanol, and then the precipitate was filtered, washed with ethanol, and dried.

8-Methyl-6-phenyl-3-(phenylamino)-4H-pyrido[1,2-b][1,2,4,5]tetrazine-9-carbonitrile (12). Brown crystals are obtained, crystallized from EtOH/DMF (70–30%); yield (71) %, mp.: 223–225 °C; FT-IR (KBr, ν, cm^{-1}): 3420(NH), 3010(CH-Ar), 2980 (CH-aliph.), 2230 (C≡N), 1619 (C=N); ^{1}H NMR: (600 MHz, $CDCl_3$) δ (ppm): 2.45 (s, 3H, CH_3), 4.03 (s, 1H, NH tetrazine), 6.77–7.49 (m, 10H, CH-aromatic), 7.82 (s, 1H, CH-pyridine), 7.86 (s, 1H, NH–Ph), ^{13}C NMR (213 MHz, DMSO-d_6) δ (ppm): 24.31(CH_3), 95.63, 96.4 (2CH-pyridine), 117.84, 117.99 (2C≡N), 118.27, 118.80, 122.03, 122.36, 124.75, 128.50, 129.42, 138.62, 141.17(phenyl C), 152.56, 154.74

(2 (C=N)-tetrazine). MS (m/z, %): 340.16($M^{+\cdot}$, 13); 339.17($M^{+\cdot}$–H, 43); 148.56(100). Anal. Calcd. for $C_{20}H_{16}N_6$ (340.14); C, 70.57; H, 4.74; N, 24.69. Found C, 70.63; H, 4.82; N, 24.75.

3,9-Dimethyl-7-phenyl-4,5-dihydropyrido[1,2-b][1,2,4,5]tetrazepine-10-carbonitrile (13). Yellow crystals are obtained, crystallized from EtOH; yield (83) %, mp.: 210–212 °C; FT-IR (KBr, ν, cm^{-1}): 3350(NH), 3009(CH-Ar), 2950(CH-aliph.), 2225 (C≡N), 1590 (C=N). ^{1}H NMR(600 MHz, $CDCl_3$) δ (ppm): 2.20 (s, 6H, $2CH_3$), 3.44 (s, 2H, CH_2-tetrazepine), 4.20 (s, 1H, NH-tetrazepine, exchangeable with D_2O), 7.18–7.40 (m, 5H, Ar–H), 7.85(s, 1H, CH-pyridine), ^{13}C NMR (213 MHz, DMSO-d_6) δ(ppm): 21.36, 22.40 ($2CH_3$), 65.41 (CH_2-tetrazepine), 87.72 (CH-pyridine), 114.20 (CH-tetrazepine), 118.20 (C≡N), 120.68, 121.48, 125.36, 129.28, 139.00 (phenyl C), 152.56, 154.74 (2 (C=N)-tetrazepine). MS (m/z, %): 277.47($M^{+\cdot}$, 34); 65.36 (100). Anal. Calcd. for $C_{16}H_{15}N_5$ (277.33); C, 69.29; H, 5.45; N, 25.25. Found C, 69.35; H, 5.38; N, 25.18.

9-Methyl-3,7-diphenyl-2,5-dihydropyrido[1,2-b][1,2,4,5]tetrazepine-10-carbonitrile (14). Orange powder is obtained, crystallized from EtOH; yield (86) %, mp.: 230–232 °C; FT-IR (KBr, ν, cm^{-1}): 3330 (NH), 3010 (CH-Ar), 2960 (CH-aliph.), 2220 (C≡N), 1605 (C=N). ^{1}H NMR (400 MHz, DMSO-d_6) δ(ppm): 2.23 (s, 3H, CH_3), 4.51(s, 2H, CH & NH-tetrazepine), 7.25–7.70 (m,10H, Ar–H), 7.76 (s, 1H, CH-pyridine), 8.10 (s, 1H, NH-tetrazepine). ^{13}C NMR (213 MHz, DMSO-d_6) δ(ppm): 24.21(CH_3), 86.41 (CH-pyridine), 104.85 (CH-tetrazepine), 117.84 (C≡N), 122.03, 122.36, 124.75, 128.57, 128.68, 129.42, 138.62 (phenyl C), 149.17 (C=N-tetrazepine). MS (m/z, %): 339.67 ($M^{+\cdot}$, 4); 336.80 ($M^{+\cdot}$–3H, 21); 78.29 (100). Anal. Calcd. for $C_{21}H_{17}N_5$ (339.40); C, 74.32; H, 5.05; N, 20.63. Found C, 74.29; H, 5.01; N, 20.69.

9-Methyl-3,4-dioxo-7-phenyl-2,3,4,5-tetrahydropyrido[1,2-b][1,2,4,5]tetrazepine-10-carbonitrile (15). Faint yellow crystals are obtained, crystallized from EtOH; yield (86) %, mp.: 200–202 °C; FT-IR (KBr, ν, cm^{-1}): 3450, 3335 (2NH), 3009 (CH-Ar), 2890 (CH-aliph.), 2220 (C≡N), 1650, 1630 (2C=O), 1600 (C=N). ^{1}H NMR (400 MHz, DMSO-d_6) δ (ppm): 2.12 (s, 3H, CH_3), 7.70 (s, 1H, CH-pyridine) 7.64–7.76 (m, 5H, Ar–H), 8.44, 8.56 (2s, 2H, 2NH-tetrazepine. ^{13}C NMR (213 MHz, DMSO-d_6) δ (ppm): 21.53 (CH_3), 82.71 (CH-pyridine), 118.22 (C≡N), 120.51, 123.74, 124.17, 127.68, 129.24, 129.41 (phenyl C), 147.74 (C=N-tetrazepine), 151.08, 152.51 (2C=O). MS (m/z, %): 293.06 ($M^{+\cdot}$, 20); 55.68 (100). Anal.Calcd. for $C_{15}H_{11}N_5O_2$ (293.29); C, 61.43; H, 3.78; N, 23.88. Found, C, 61.38; H, 3.72; N, 23.80.

1-((3,4-Dimethoxybenzylidene)amino)-2-hydrazono-4-methyl-6-phenyl-1,2-dihydro- pyridine-3-carbonitrile (16). Orange crystals are obtained; crystallized from EtOH; yield (88) %, mp.: 246–248 °C; FT-IR (KBr, ν, cm^{-1}): 3450, 3340 (NH_2), 3010 (CH-Ar), 2950 (CH-aliph.), 2225 (C≡N), 1600(C=N). ^{1}H NMR (600 MHz, DMSO-d_6) δ (ppm): 2.15 (s, 3H, CH_3), 3.44 (s, 3H, OCH_3), 3.70 (s, 3H, OCH_3), 5.36 (s, 2H, NH_2, exchangeable with D_2O), 7.07–7.42 (m, 8H, Ar–H), 7.40 (s, 1H, CH-pyridine), 7.69 (s, 1H, CH=N–). Anal. Calcd. for $C_{22}H_{21}N_5O_2$ (387.44); C, 68.20; H, 5.46; N, 18.08. Found, C, 68.14; H, 5.54; N, 18.02.

Biological activities. *NCI anticancer activity screening.* The preliminary anticancer screening for novel fused pyridine derivatives (**2**–**16**) was performed in the Developmental Therapy Program of the National Cancer Institute (NCI) in the United States. In accordance with the NCI, Bethesda, Drug Evaluation Branch procedure (http://dtp.nci.nih.gov), the twelve derivatives **2**, **4**, **5**, **7**–**10,** and **12**–**16** were chosen and tested for initial in vitro one dose anticancer testing at 10^{-5} M concentration against full NCI 60 cell line screens indicating nine various types of cancer comprising renal cancer, leukaemia, melanoma, prostate cancer, non-small cell lung cancer, ovarian cancer, CNS cancer, breast cancer. The results of each tested compound (**2**, **4**, **5**, **7**–**10**, and **12**–**16**) were provided as a mean chart of the growth percentage of the treated cells as compared to the control, which reveals both inhibitory values (between 0 and 100) and toxicity values (less than 0). The COMPARE tool was used to examine the single-dose evaluation findings of all chosen compounds against sixty cancer cell lines. As previously stated[20], every molecule supplied for the NCI-60 Cell screen is examined at a single high dosage (10^{-5} M).

Protein preparation and molecular docking work. The docking investigation was carried out using the computer software Molecular Operating Environment (MOE) version 2015.10[21], Chemical Computing Group Inc., Montreal, Quebec, Canada. The docking technique was carried out as previously reported[22]. The 3-dimensional (3D) structure of Janus Kinase (Jak2) with PDB ID: **4P7E** was obtained through the link (https://www.rcsb.org/structure/4P7E) on the Protein Data Bank site. Using the program's default parameters, the co-crystallized ligand was re-docked in its original protein structure. Interactions of the amino acids, affinities by bond strength, and hydrogen bond lengths were illustrated in Table 1.

Designing and optimization of more potent fused pyridine derivatives. Molecular orbital and electrostatic characteristics are frequently calculated using quantum mechanical techniques. The Gaussian 09 software program was used to complete the calculations, which used density functional theory (DFT)[23]. DFT with Beck's (B)[24] three-parameter hybrid models and Lee, Yang, and Parr's (LYP)[25] association function under 6-31G (d,p) basis set was used to optimize and forecast the molecular orbital features of the more active fused pyridine derivatives (**4**, **8**, and **9**). At the same level of theory, the highest occupied molecular orbital (HOMO) and the lowest unoccupied molecular orbital (LUMO) were counted as frontier molecular orbital characteristics. The HOMO–LUMO energy gap was computed for each of the more powerful derivatives.

	Compounds[a]											
Subpanel/tumour cell lines	**2**	**4**	**5**	**7**	**8**	**9**	**10**	**12**	**13**	**14**	**15**	**16**
Leukemia												
CCRF-CEM	–	–	–	–	–	–	–	–	–	–	–	–
HL-60(TB)	–	–	–	–	–	–	–	–	–	–	–	–
K-562	–	12.50	–	19.06	11.47	–	–	–	–	–	–	–
MOLT-4	–	–	–	–	–	–	–	–	–	–	–	–
RPMI-8226	–	**22.45**	13.43	11.43	**29.42**	**51.58**	–	–	–	–	–	–
SR	–	–	–	9.30	–	–	–	–	–	–	–	–
Non-small cell lung cancer												
A549/ATCC	–	–	–	–	–	–	–	–	–	–	–	–
EKVX	–	–	–	–	–	–	16.39	–	–	–	–	–
HOP-62	16.88	**23.38**	12.88	**30.19**	**29.39**	**20.17**	**22.28**	18.57	13.10	14.43	16.16	**22.80**
HOP-92	NT	NT	NT	NT	NT	NT	NT	NT	NT	NT	NT	NT
NCI-H226	–	–	–	–	–	11.58	–	–	–	–	–	–
NCI-H23	–	–	–	–	–	–	–	–	–	–	–	–
NCI-H322M	–	–	–	8.09	–	–	–	–	–	–	–	–
NCI-H460	–	–	–	–	–	–	–	–	–	–	–	–
NCI-H522	10.14	19.05	13.32	16.19	**24.14**	12.55	8.83	10.63	–	–	–	–
Colon cancer												
COLO 205	–	–	–	–	–	–	–	–	–	–	–	–
HCC-2998	–	–	–	–	–	–	–	–	–	–	–	–
HCT-116	–	9.85	–	–	14.71	**77.94**	–	–	–	–	–	–
HCT-15	–	–	–	–	–	–	–	–	–	–	–	–
HT29	–	–	–	–	–	–	–	–	–	–	–	–
KM12	–	–	–	–	10.42	-	–	–	–	–	–	–
SW-620	–	–	–	–	–	8.07	–	–	–	–	–	–
CNS cancer												
SF-268	–	–	–	–	–	–	–	–	–	–	–	–
SF-295	–	–	–	–	14.91	9.57	–	–	–	–	–	–
SF-539	–	–	–	–	–	–	–	–	–	–	–	–
SNB-19	–	10.40	8.87	8.94	14.40	12.79	–	–	–	–	–	–
SNB-75	NT	NT	NT	NT	NT	NT	NT	NT	NT	NT	NT	NT
U251	–	–	–	–	–	9.37	–	–	–	–	–	–
Melanoma												
LOX IMVI	–	–	–	8.68	–	8.76	–	–	–	–	–	–
MALME-3M	–	–	9.41	–	14.76	–	16.30	–	–	–	–	8.69
M14	–	–	–	–	–	–	–	–	–	–	–	–
MDA-MB-435	–	–	–	–	–	–	–	–	–	–	–	–
SK-MEL-2	–	–	–	–	–	–	–	–	–	–	–	–
SK-MEL-28	–	–	–	–	–	–	–	–	–	–	–	–
SK-MEL-5	–	–	–	–	–	–	–	–	–	–	–	–
UACC-257	–	–	–	–	9.97	–	–	–	–	–	–	–
UACC-62	–	**21.71**	–	**22.82**	**28.57**	19.56	12.73	–	–	–	–	9.64
Ovarian cancer												
IGROV1	–	15.09	–	–	–	10.62	–	–	–	–	–	–
OVCAR-3	–	–	–	–	–	–	–	–	–	–	–	–
OVCAR-4	–	9.96	–	–	13.10	–	–	–	–	–	–	–
OVCAR-5	–	–	–	–	–	–	–	–	–	–	–	–
OVCAR-8	–	–	–	–	–	–	–	–	–	–	–	–
NCI/ADR-RES	–	–	–	–	–	–	–	–	–	–	–	–
SK-OV-3	–	8.53	–	11.98	**36.25**	12.68	13.42	10.36	–	–	–	17.88
Renal cancer												
786-0	–	–	–	–	–	–	–	–	–	–	–	–
A498	–	–	–	–	–	–	–	–	–	–	–	–
ACHN	–	8.16	–	–	–	–	–	–	–	–	–	–
CAKI-1	–	16.21	–	16.91	16.39	16.77	13.41	–	–	–	–	15.57
Continued												

Subpanel/tumour cell lines	Compounds[a]											
	2	4	5	7	8	9	10	12	13	14	15	16
RXF 393	–	–	–	–	–	–	–	–	–	–	–	–
SN12C	–	–	–	–	–	–	–	–	–	–	–	–
TK-10	13.75	–	–	–	–	–	–	–	–	–	9.11	-
UO-31	9.31	**32.07**	**24.74**	**28.36**	**24.10**	**36.84**	**34.48**	**25.30**	10.78	8.76	9.83	**27.71**
Prostate cancer												
PC-3	–	8.83	–	**21.02**	**23.28**	9.91	–	–	–	–	–	18.14
DU-145	–	–	–	–	–	–	–	–	–	–	–	–
Breast cancer												
MCF7	NT	NT	NT	NT	NT	NT	NT	NT	NT	NT	NT	NT
MDA-MB- 231/ATCC	–	13.08	–	15.43	13.78	15.35	17.01	–	–	–	–	10.11
HS 578 T	–	–	–	–	8.14	9.27	13.16	–	–	–	–	–
BT-549	–	–	–	–	–	–	–	–	–	–	–	11.22
T-47D	–	**32.30**	9.75	**28.31**	18.61	19.37	12.09	–	–	–	–	15.02
MDA-MB-468	–	–	–	–	–	–	–	–	–	–	–	–

Table 1. In vitro anticancer screening results of compounds **2, 4, 5, (7–10) and (12–16)** against sixty human tumour cell lines with single dose assay (10^{-5} M concentration). Data was provided as cell growth inhibition percentage. [a]Only GI % higher than 8% are shown. *NT* not tested. Significant values are in [bold].

In silico physicochemical properties, drug-likeness, and pharmacokinetics profiles of most active compounds 4, 8, and 9 compared to the reference 2HB. Drug development is incomplete unless the pharmacokinetic parameters of drug candidates are evaluated during the primary screening stage because some drug candidates do not act therapeutically due to insufficient pharmacokinetic characteristics. This process may result in better hits and less late-stage abrasion of drug candidates. To identify the physicochemical properties, drug-likeness, and ADME profile, "absorption, distribution, metabolism, and excretion" were calculated hypothetically based on SwissADME online software [www.SwissADME.ch].

Discussion of the results

Chemistry. As reported, the cyclocondensation of 2-cyanoacetohydrazide with benzoyl acetone in a slightly alkaline medium afforded the dihydropyridine-3-carbonitrile (**1**)[19] as the primary entry material for the synthesis of bridgehead pyrido[1,2,4,5]tetrazine and pyrido-azepines with one ring joint nitrogen atom.

The treatment of building block **1**[19] with cyanoguanidine yielded the fused triazolopyridine **2** in good yield, rather than the predictable 2,4-diamino-9-methyl-7-phenylpyrido[1,2-*b*][1,2,4,6]tetrazepine-10-carbonitrile (Fig. 1). Compound **2** is produced due to the elimination of the water molecule, followed by intramolecular cyclization by removing the NH_3 molecule. The appearance of an NH proton signal at 3.80 ppm exchangeable with D_2O in the ^{1}H-NMR spectrum, and a new carbon signal corresponding to the cyano group at 118.93 ppm in the ^{13}C NMR spectrum, affirmed the structure of compound **2**.

Additionally, substrate **1**[19] was alkylated with chloroacetone, furnishing the open-chain product **3**, which was further subjected to cyclocondensation upon fusion with phenylhydrazine to form the cyclized [1,2,4,5] tetrazepine analogue **4**. The structures of these compounds have been verified by their spectral data (See the Supplementary file).

The fused heterocyclic system (6:7:6) with a single ring connection atom of nitrogen was synthesized through the fusion of the key compound **1**[19] with the binucleophilic anthranilic acid at 140–160 °C, affording the biologically active benzo[*e*]pyrido[1,2,4]triazepine derivative **5** (Fig. 1).

Figure 2 depicts the synthesis of pyrido[1,2,4,5]tetrazines via two pathways: [3 + 3]-and [5 + 1]-annulations. The first pathway was developed under solvent-free conditions via [3 + 3] cyclocondensation of **1**[19] and the binucleophilic thiosemicarbazide. The reaction gave the corresponding 3-aminopyrido[1,2-*b*][1,2,4,5]tetrazine **7** in 89% yields. The reaction mechanism of compound **7** was hypothesized to proceed via the elimination of both H_2O and H_2S molecules as follows: initial condensation of the carbonyl functionality of compound **1** with the primary amine group of the thiosemicarbazide to give an intermediate by removal of a water molecule, followed by ring closure via removal of a hydrogen sulphide molecule to give the target compound **7**, which can be tautomerized to its tautomeric form, as illustrated in Fig. 2. The ^{1}H-NMR spectrum of compound **7** recorded two singlet signals at 6.43 and 12.60 ppm exchangeable with D_2O, attributed to amine and tetrazine-NH, respectively. It is important to note that the fusion of substrate **1**[19] with a different reactive reagent, hydrazinecarbonitrile, produced the tautomer of compound **7** through a different mechanism and resulted in 3-imino-2*H*-pyrido[1,2-b][1,2,4,5]tetrazine **6** in a 67% yield (Fig. 2). A reaction mechanism is postulated with an initial nucleophilic attack on the carbonyl functional group of compound **1** by the amino nitrogen of the hydrazinecarbonitrile, providing an intermediate by the elimination of a water molecule. The intermediate then undergoes cyclization by attacking the primary amino group on the nitrile carbon, leading to the formation of compound **6**.

The presence of a primary amine functionality in the ortho position to tetrazine-NH opens the way for subsequent chemical modification of tetrazines. Thus, tetrazine derivative **7** was a good substrate for synthesizing

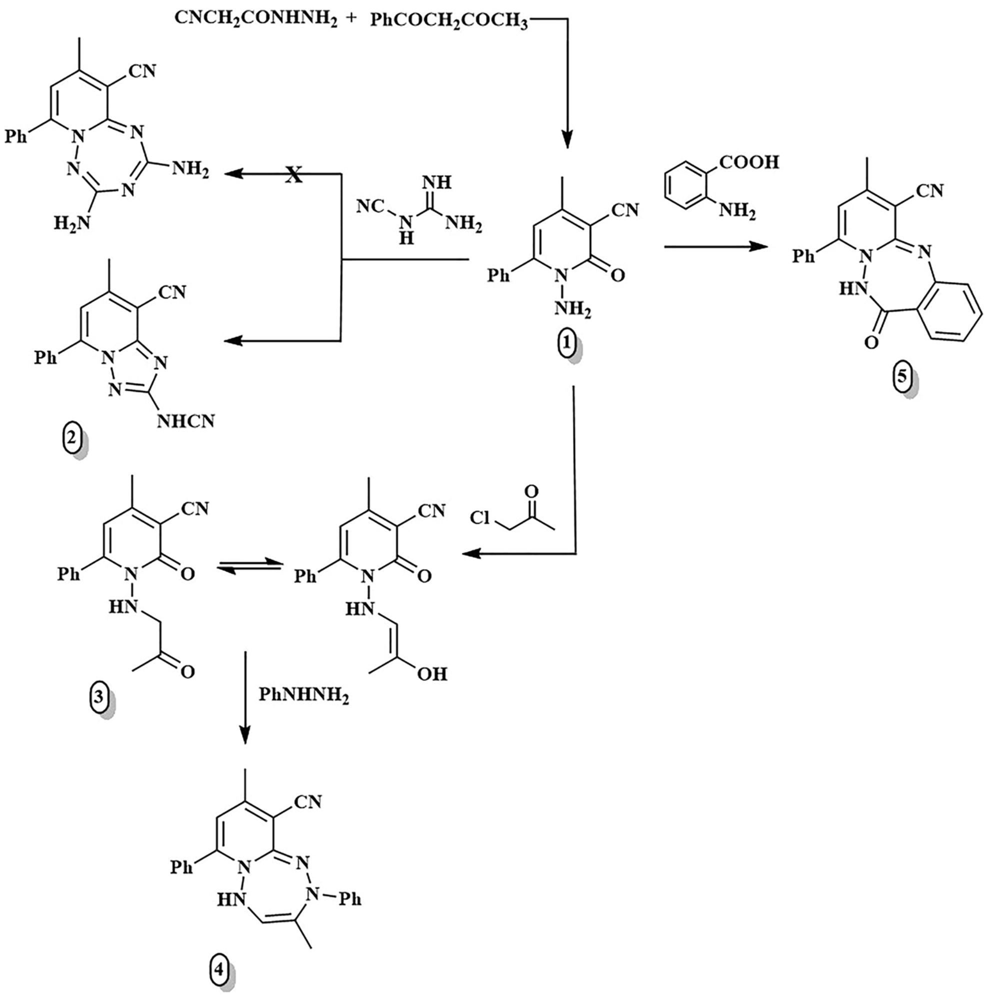

Figure 1. Synthesis of compounds **2**–**5**.

a wide range of five- and six-membered heterocycles with high yields via [3 + 2]-and [3 + 3]-cyclocondensation reactions with 1,2- and 1,3-synthons, respectively. The fused heterocyclic system (6:6:6) with two nitrogen ring connections was obtained by fusing compound **7** with a 1,3-dicarbonyl compound, such as diethyl malonate, resulting in the respective dihydropyrimidinone derivative **8**. The formation of the pyrimidine ring was confirmed through ^{13}C-NMR with signals at δ 43.47, 160.74, and 163.55 ppm assignable for CH_2-pyrimidine and two amidic carbonyl carbons, respectively (Fig. 2). While tricyclic imidazo[1,2-*b*]pyrido[1,2-*e*][1,2,4,5]tetrazine analogues **9** and **10** were formed through the treatment of compound **7** with active methylene compound as phenacyl bromide and 1,2-di electrophilic diethyl oxalate; respectively. Compounds **9** and **10**'s structures were determined using spectroscopic data (see the Supplementary file).

Another important starting point was hydrazone derivative **11**, formed by hydrazinolysis of the substrate **1**[19] with an equimolar amount of hydrazine hydrate in the absence of solvent (Fig. 3). The latter compound was affirmed by the appearance of a new deuterium oxide exchangeable singlet in ^{1}H NMR at δ 5.49 ppm due to =N–NH_2 protons. In addition, the ^{13}C NMR spectrum assured the absence of a carbonyl signal as well as the existence of a signal at δ 146.49 ppm correlated to C = N. Compound **11** was utilized as another way for the preparation of [1, 2, 4, 5]tetrazine and derivatives of [1, 2, 4, 5]tetrazepine via [5 + 1]- and [5 + 2]-annulation, respectively. The fusion of hydrazone derivative **11** with one carbon compound as phenylisothiocyanate was the second pathway for synthesizing pyrido[1,2,4,5]tetrazine **12** via [5 + 1]-annulation. The mechanism of compound **12** was expected to take place first via Michael's addition of the primary amine of **11** to the electron-deficient double bond in PhNCS, generating a Michael-type open-chain adduct (thiocarbamoyl intermediate) that underwent a cyclocondensation reaction with H_2S removal. Compound **12** displayed characteristic ^{1}H-NMR signals at δ 7.86 ppm and 4.03 ppm corresponding to NH-phenyl and NH-tetrazine, respectively, whereas the ^{13}C NMR demonstrated signals at 152.56 and 154.74 ppm due to C=N-tetrazine carbons. On the other hand, the catalyst- and solvent-free [5 + 2]-cyclocondensation was applied to synthesize pyrido[1,2-*b*][1,2,4,5]tetrazepine derivatives **13** and **14** by fusing the key starting material **11** with α-halo carbonyl compounds, namely chloroacetone and phenacyl bromide, respectively at 140–160 °C. Additionally, 2,3,4,5-tetrahydropyrido[1,2-*b*][1,2,4,5]tetrazepine-3,4-dione **15** was easily obtained in high yield by treating hydrazone derivative **11** with diethyl oxalate. ^{1}H-NMR

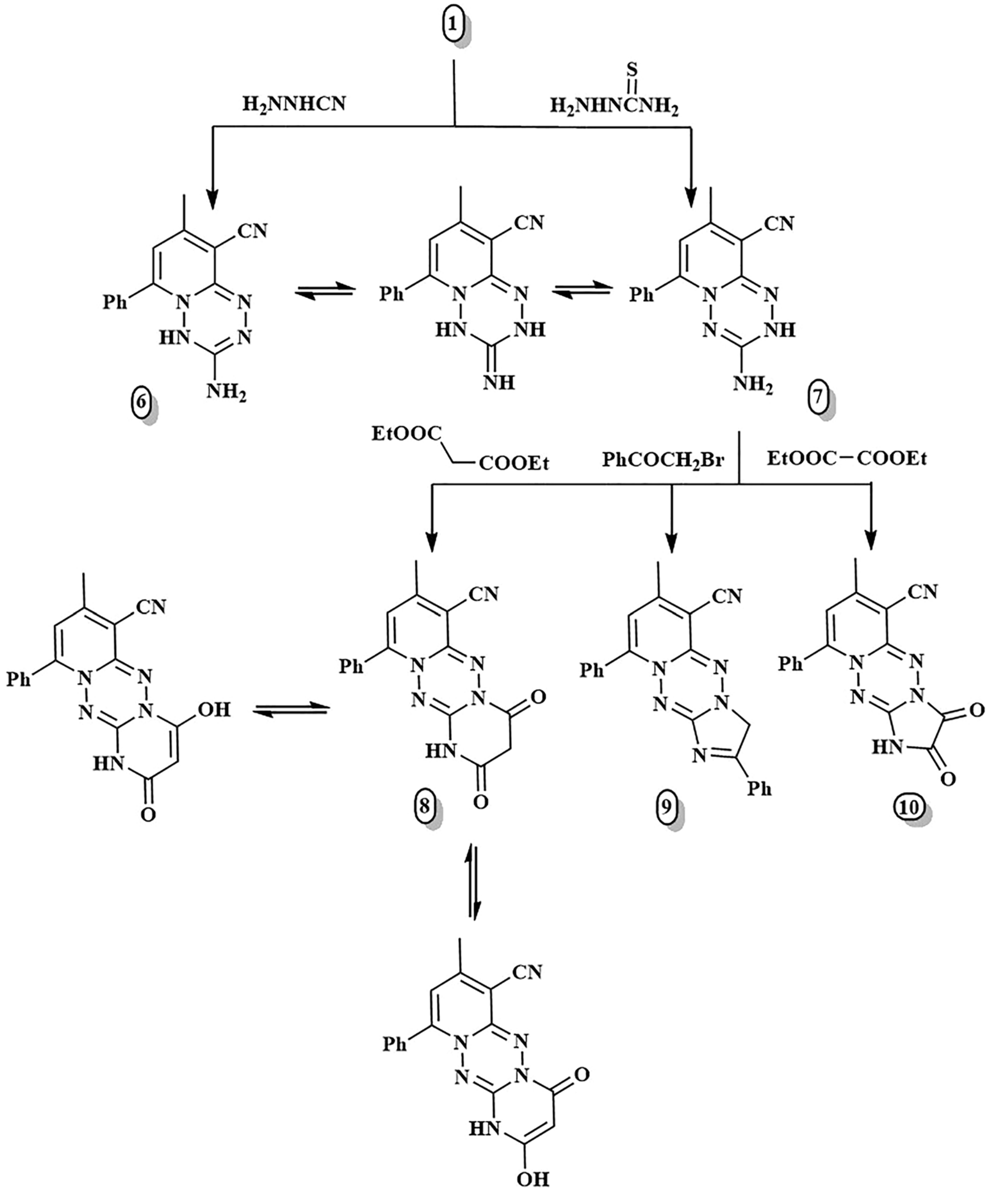

Figure 2. Synthesis of compounds **6**–**10**.

demonstrated new signals at 8.44 and 8.56 ppm for two tetrazepine-NH protons, respectively, whereas ^{13}C-NMRR displayed distinguishable signals at 151.08 and 152.51 ppm for two C=O carbons. Finally, Schiff base **16** can be formed through the condensation of compound **11** with 3,4-dimethoxybenzaldehyde. The ^{1}H-NMR spectrum of **16** showed a singlet signal at 7.69 ppm due to the (CH=N–) proton.

Biological activity.

NCI screening of anticancer activity. Preliminary single high dose screening at 10^{-5} M concentration. Twelve synthesized derivatives were tested for in vitro anticancer activity; some showed modest activity in numerous cancer cell lines, while others showed impact against further than one cancer cell line. Table 1 shows the most sensitive cell lines' growth inhibition percentages (GI %).

More specifically, compounds (**4**, **5**, **7**, **8**, **10**, **12**, and **16**) showed moderate activity with a mean GI% range (of 21.02–36.25) % against several forms of cancers, including Leukemia (RPMI-8226), non-small cell lung cancer (HOP-62 & NCI-H522), Melanoma (UACC-62), Renal cancer (UO-31), Brest cancer (T-47D), Prostate cancer (PC-3), and Ovarian Cancer (SK-OV-3) (Fig. 4).

Among all tested compounds, **9** demonstrated strong anticancer cell line efficacy against Leukemia-RPMI-8226 (GI% = 51.58%) and Colon cancer-HCT116 (GI% = 77.94%). On the other hand, compound **9** inhibited various cell lines in a mild to moderate manner with a mean GI% range (of 8.07–36.84) % (Fig. 5a).

Compounds **2** and **13**–**15** were ineffective against the bulk of the subpanels of cancer cell lines. They revealed a weak effective anticancer efficacy against certain cell lines, such as Non-small cell lung cancer (HOP-62 &

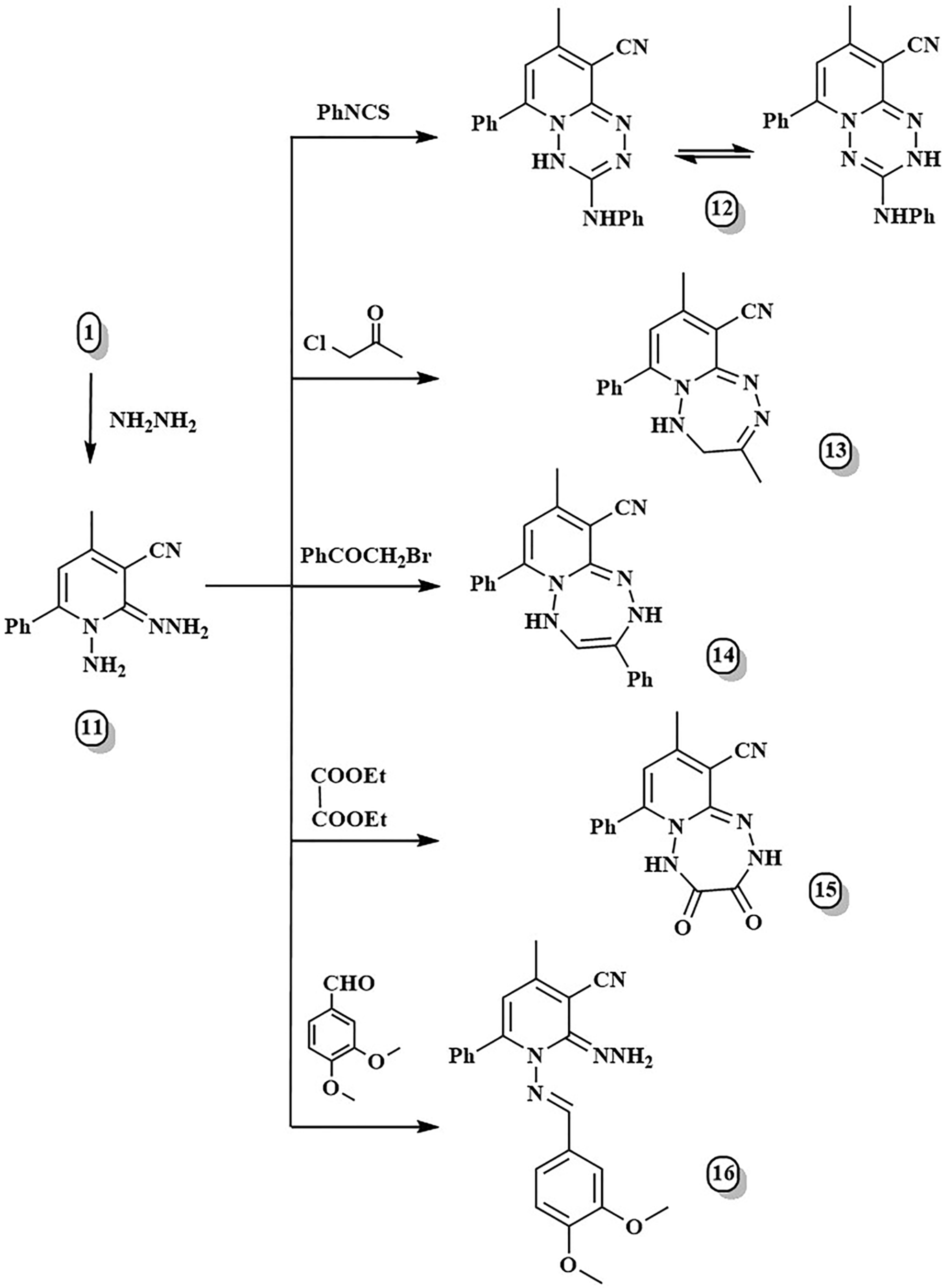

Figure 3. Synthesis of compounds **11**–**16**.

NCI-H522) and Renal cancer (UO-31 & TK-10) with GI% range (8.76–16.88)% (Fig. 5b). The screening findings revealed that **4, 8,** and **9** exhibited the maximum activity in some of the cell lines in the current study.

Analysis of molecular docking. The conjugates (**4**, **8**, and **9**) exceeded all other produced fused pyridine derivatives in terms of biological activity against various cancer cell lines. To examine their binding mechanism and non-bonding effects, we did a molecular docking versus Janus Kinase (Jak2) (PDB: 4P7E). The docking process was first confirmed by re-docking the co-crystallized ligand **2HB** (N-(5–4)[(1,1-dioxidothiomorpholin-4-yl) methyl]phenyl[1,2,4]triazolo[1,5-*a*]pyridin-2-yl)cyclopropane carboxamide) at the enzyme's active sites. **2HB** has an energy score (S) = − 7.45 kcal/mol and showed one H-bond as Lys 882 with SO_2 group and three arene-H interactions with Gly 856, Ser 936, and Leu 855 residues (Fig. 6).

Table 2 revealed that compounds **4** and **9** have an energy score (S) = − 7.24 and − 7.25 kcal/mol, respectively, close to that of the **2HB** ligand. Compound **4** can establish two H-bonds as Leu 932 with CN group and one hydrogen bond between the CH_3 group and the residue Met 929. On the other hand, Leu 855 showed three

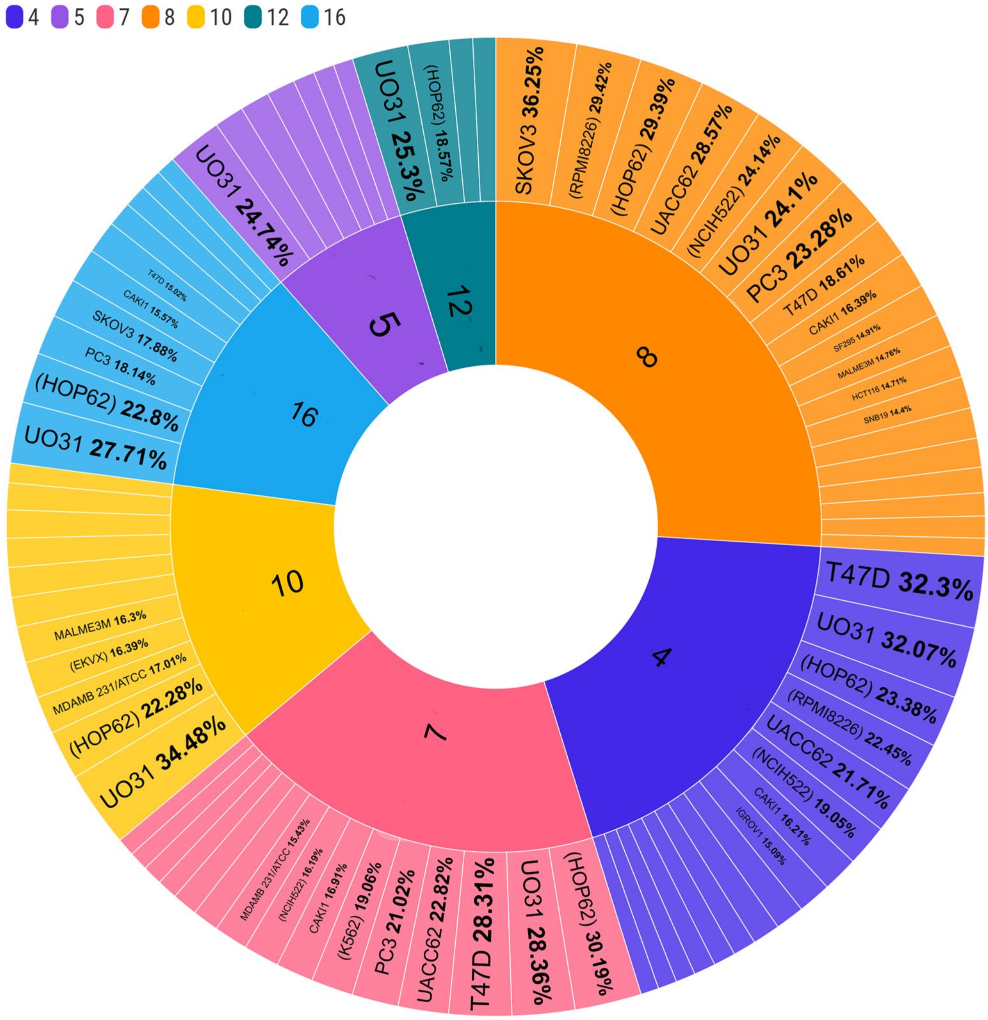

Figure 4. Sunburst chart represents **GI%** higher than **15%** for compounds **4**, **5**, **7**, **8**, **10**, **12**, and **16** against cancer cell lines of the nine tumour panels.

H-arene contacts with the benzene and tetrazepine ring of compound **4**, also the pyridine nucleus produced four arene-H interactions with Val 863 and Leu 983 amino acids (Fig. 7). Compound **8** had an energy score (S) = −6.56 kcal/mol, two H-bonds were observed between CN group and the residue Leu 932 and one H-bond formed between Leu 855 and N of tetrazine ring, also, Leu 855 showed two H-arene interaction with tetrazine ring. In addition, the pyridine ring of **8** was oriented in close contact with Leu 983 and Val 863, forming four arene-H interactions (Fig. 8). Finally, compound **9** established one hydrogen bond as Val 911 with CN group and eight arene-H contacts as benzene ring with Leu 855, pyridine ring with (Ser 936, Leu 855 & Val 863) and tetrazine ring with (Val 863 & Leu 983) (Fig. 9).

Analysis of frontier molecular orbitals. The most fundamental orbitals in molecules are the frontier molecular orbitals, which are used to determine kinetic stability and chemical reactivity. The highest occupied molecular orbital (HOMO) and the lowest unoccupied molecular orbital (LUMO) are the names given to the Frontier molecular orbitals. Figure 10 shows that the HOMO orbitals are less localized than the LUMO orbitals. Electronic absorption is the transition from the ground state to the first excited state and is best defined by the excitation of an electron from HOMO to LUMO[26]. Kinetic stability rises when the HOMO–LUMO gap widens. As a result, moving electrons from the stable state HOMO to the excited state LUMO needs more energy. For compounds **4**, **8**, and **9**, the majority of the HOMO is placed mainly on the pyridine ring and the fused triazepine or triazine rings, with a little contribution from the phenyl ring connected to triazepine nitrogen atom as in compound **4**. Compounds **4** and **8** have LUMOs localized on the pyridine ring, nitrogen atoms of the fused ring, and the phenyl ring attached to pyridine. In contrast, compound **9** has LUMOs localized on the pyridine ring, 4-phenyl imidazole moiety, and nitrogen atoms of fused triazine. Table 3 displays orbital energy and dipole moment values calculated for the selected compounds (**4**, **8, 9**) and **2HB**. The dipole moments of the more potent conjugates and **2HB** were investigated, revealing that the compounds have large dipole moments in the order **8** > **2HB** < **4** > **9**. Although, compounds **4**, **8,** and **9** have an energy gap of 0.1052, 0.1153, and 0.0875 eV,

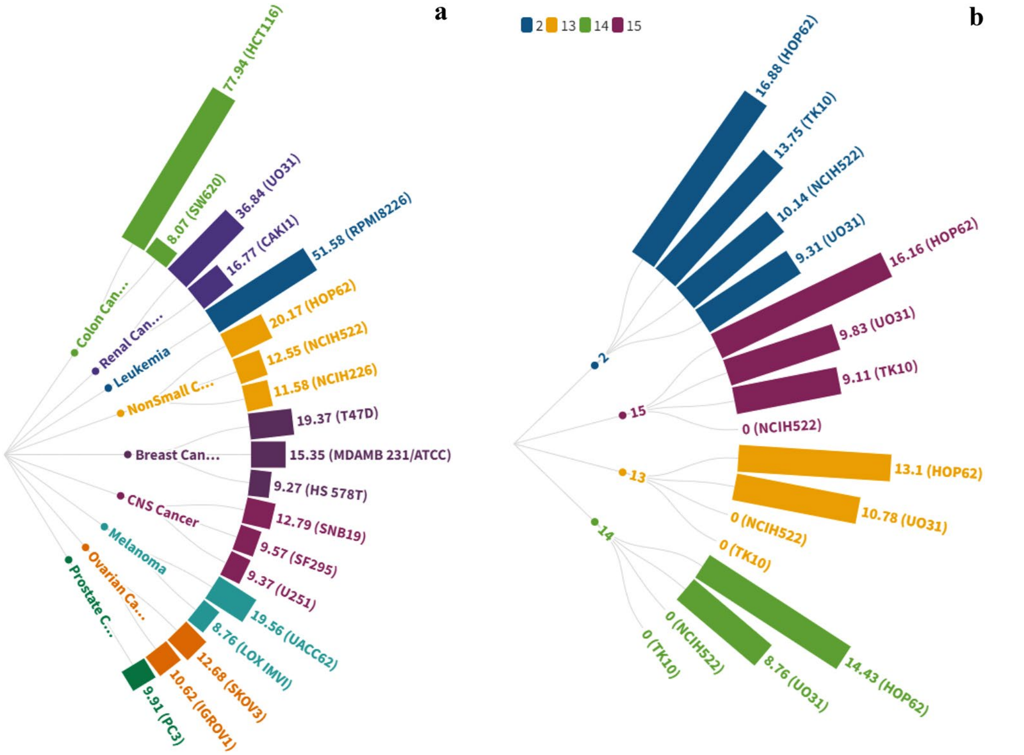

Figure 5. Radial bar chart represents (**a**): **GI%** of compound **9** against cancer cell lines of the nine tumour panels. (**b**): **GI%** of compounds (**2**, **13**, **14**, and **15**) against cancer cell lines of the nine tumour panels.

respectively, which are smaller than that of **2HB** (0.1594 eV) (Fig. 10). As a result, these chemicals (**4**, **8** and **9**) may enable higher interaction with high dipole moment species, particularly in biological systems.

The electrostatic potential of molecules (MEP). The molecular electrostatic potential (MEP) aids in interpreting the biological recognition phase and hydrogen bonding connections[27]. The MEP map of compounds (**4**, **8**, **9**) and **2HB** was generated using the B3LYP with the basis set 6-31G optimized outputs (Fig. 11). MEP was computed to identify the reactive functional groups for electrophilic and nucleophilic reactions in terms of colour grading of the optimized structure of compounds (**4**, **8**, **9**) and **2HB** (Fig. 12). The red colour represents the maximum negative area, which suggests a desirable site for electrophilic attacks, the blue colour represents the largest positive area, which indicates a favourable site for nucleophilic attacks, and the green colour represents zero potential regions.

In silico ADME studies. Physicochemical properties and drug-likeness. A bioinformatics study was performed on the most active compounds **4, 8**, and **9** to predict their physicochemical and drug-likeness properties. The physicochemical properties for oral bioavailability, which include (size: MW between 150 and 500 g/mol, lipophilicity: Log P between − 0.7 and + 5.0, polarity: TPSA between 20 and 140 Å, flexibility: no more than 10 rotatable bonds, and solubility: log S not higher than 6) demonstrated that all examined compounds have good physicochemical properties similar to the reference 2HB (Table 4). Furthermore, compounds should meet the following criteria under the Lipinski rule of five, which indicates that drugs have good absorption and bioavailability: M.wt. ≤ 500, log P ≤ 5, HBD ≤ 5, and HBA ≤ 10, as shown in Table 4. The examined compounds **4, 8,** and **9** had good values for all of the rule principles with potential drug-like properties, indicating that these compounds may meet cell membrane permeability and bioavailability requirements.

The ADME profile. Further on, the SwissADME Web tool was used to investigate the pharmacokinetics of compounds **4, 8,** and **9,** as well as the reference 2HB. According to the Boiled-egg model[28], all compounds had high gastrointestinal absorption (GI), indicating their ability to easily absorb through the intestinal wall. Compounds **4** and **9** were also shown to cross the blood–brain barrier (BBB), which may be useful in anticancer drugs targeting the CNS. In contrast, compound **8** was distinguished by a lack of BBB permeability, indicating the absence of CNS drawbacks like the reference 2HB (Table 5). Furthermore, compounds **4, 8,** and **9** were shown not to bind to P-glycoproteins, in contrast to the reference 2HB.

Moreover, the compounds' interactions with cytochromes P450 (CYP) in the liver, which is the main factor for drug elimination via metabolic biotransformation, have been investigated. Compounds **4** and **9** are indicated to inhibit four and three of the five major isoforms of hepatic cytochrome P-450 (CYP), respectively, and should be administered at time intervals when other drugs are prescribed to avoid potential drug interactions, similar

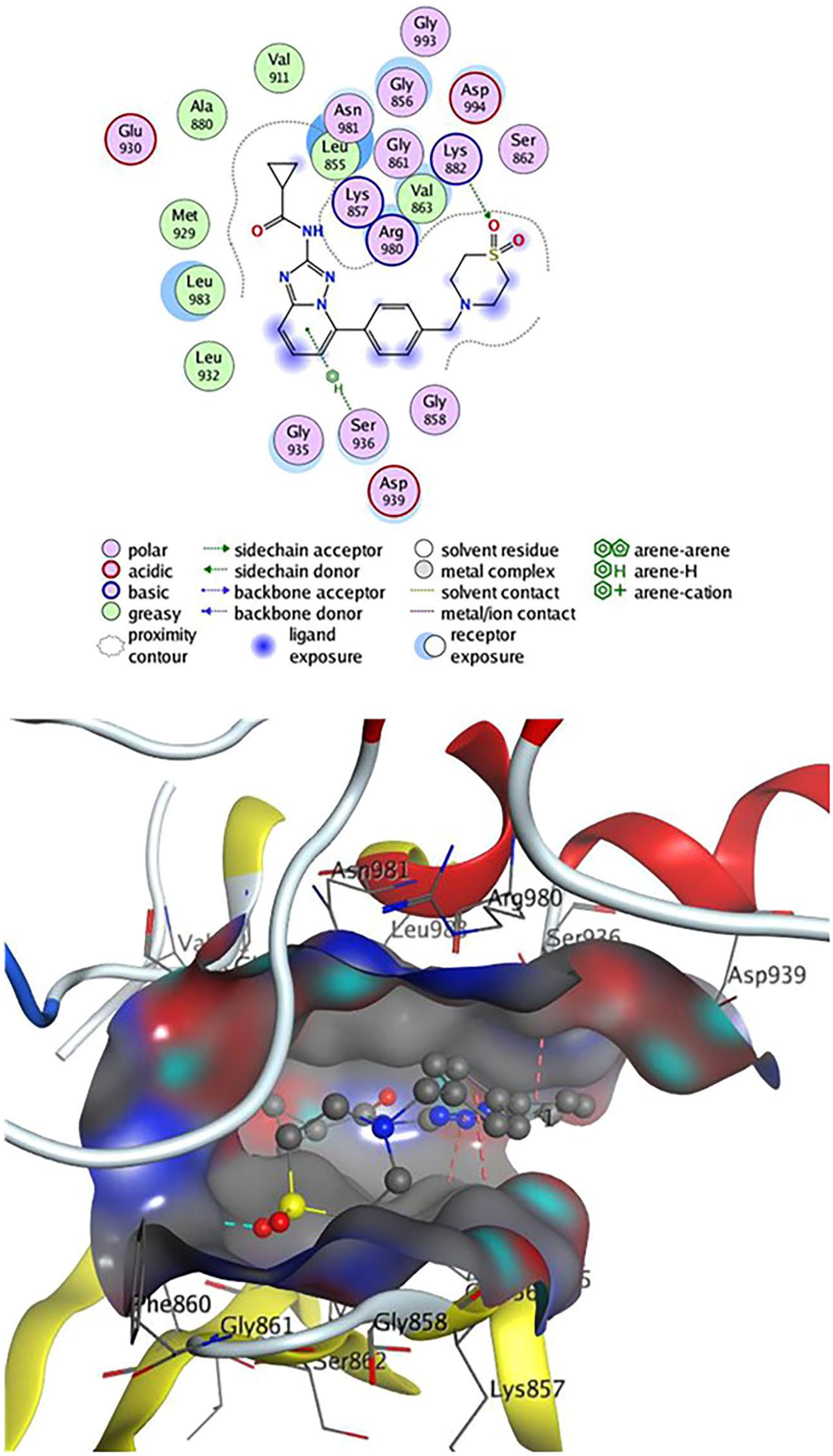

Figure 6. 2D& 3D interaction of **2HB** in the active site of Janus kinase **Jak2** (PDB ID: **4P7E**). Hydrogen bonds are displayed in cyan & H-pi-bonds are in dark pink.

Janus Kinase (4P7E)						
Comp	**Score**	**Affinity bond strength (Kcal/mol)**	**Affinity bond length (in A° from the main residue)**	**Amino acids**	**Ligand functional group**	**Interaction**
4	−7.24	−0.3	2.78	Leu 932	C≡N	H-acceptor
		−3.6	3.23	Leu 932	C≡N	H-acceptor
		−0.2	3.91	Met 929	CH_3	H-donor
		−0.4	3.56	Leu 855	Benzene ring	pi-H
		−0.2	4.55	Leu 855	Tetrazepine ring	pi-H
		−1.3	3.86	Leu 855	Tetrazepine ring	pi-H
		−0.8	4.00	Val 863	Pyridine ring	pi-H
		−0.5	4.54	Val 863	Pyridine ring	pi-H
		−0.7	3.68	Leu 983	Pyridine ring	pi-H
		−0.2	4.19	Leu 983	Pyridine ring	pi-H
8	−6.56	−0.3	2.79	Leu 932	C≡N	H-acceptor
		−3.3	2.26	Leu 932	C≡N	H-acceptor
		−0.2	3.92	Leu 855	N of tetrazine ring	H-acceptor
		−0.3	4.66	Leu 855	Tetrazine ring	pi-H
		−1.5	4.14	Leu 855	Tetrazine ring	pi-H
		−0.2	4.12	Leu 983	Pyridine ring	pi-H
		−0.5	3.56	Leu 983	Pyridine ring	pi-H
		−0.4	4.63	Val 863	Pyridine ring	pi-H
		−0.8	4.14	Val 863	Pyridine ring	pi-H
9	−7.25	−0.2	3.93	Val 911	C≡N	H-acceptor
		−0.5	4.75	Leu 855	Benzene ring	pi-H
		−0.8	3.79	Ser 936	Pyridine ring	pi-H
		−0.3	4.09	Leu 855	Pyridine ring	pi-H
		−0.3	4.59	Leu 855	Pyridine ring	pi-H
		−0.6	4.45	Val 863	Pyridine ring	pi-H
		−0.5	4.12	Val 863	Tetrazine ring	pi-H
		−1.0	4.09	Val 863	Tetrazine ring	pi-H
		−0.2	4.26	Leu 983	Tetrazine ring	pi-H
2HB	−7.45	−1.1	3.31	Lys 882	SO_2	H-acceptor
		−0.3	4.65	Gly 856	Benzene ring	pi-H
		−0.6	4.24	Ser 936	Pyridine ring	pi-H
		−0.3	4.59	Leu 855	Triazole ring	pi-H

Table 2. Docking results of compounds **4**, **8**, **9,** and **2HB** ligand inside Janus Kinase **Jak2** (PDB ID: **4P7E**) active spots.

to the reference 2HB, which is indicated to inhibit both CYP2C9 and CYP3A4. On the other hand, compound **8** is expected to inhibit none of the cytochrome P-450 (CYP) isoforms in the liver, making it safe to use together with other drugs (Table 5).

Conclusion

The fusion technique was applied for synthesizing several novel bioactive nitrogen-rich heterocycles, including pyrido-annelated [1, 2, 4, 5]tetrazines, [1, 2, 4]triazepine, and [1, 2, 4, 5]tetrazepines, with yields ranging from 67 to 89%. Additionally, molecules **4**, **8**, and **9** had the highest anticancer effect against many cancer cell lines. Furthermore, compounds **4**, **8**, and **9** have low HOMO–LUMO energy gaps, so that they may become more reactive than the **2HB** ligand. Moreover, the docked complex of analogues **4**, **8**, and **9** with **4P7E** had a higher binding affinity. The MEP study findings revealed the most negative and positive surface areas of the examined conjugates, allowing us to predict potential hydrogen bonding sites. Finally, In silico investigations of the compounds produced encouraging results, including strong GI absorption, good oral bioavailability, and perfect physicochemical features, indicating their potential as attractive medicinal targets "Supplementary Information".

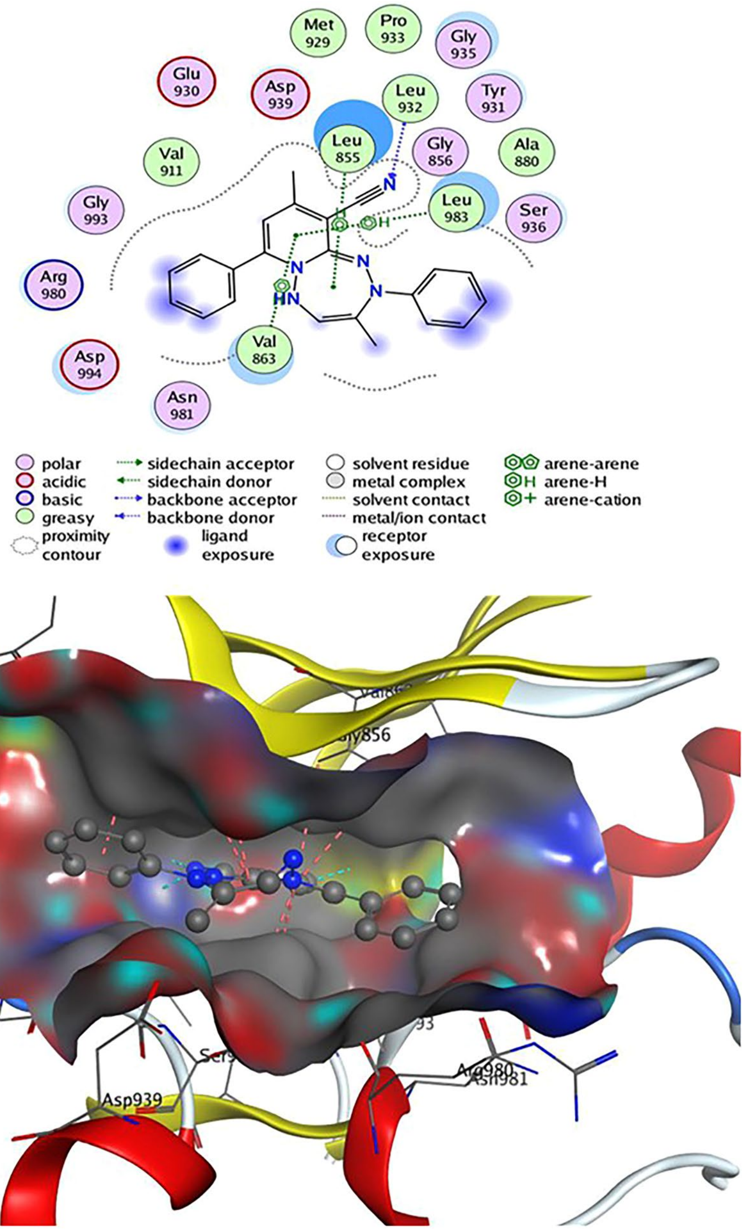

Figure 7. 2D& 3D interaction of **4** in the active site of Janus kinase **Jak2** (PDB ID: **4P7E**). Hydrogen bonds are displayed in cyan & H-pi-bonds are in dark pink.

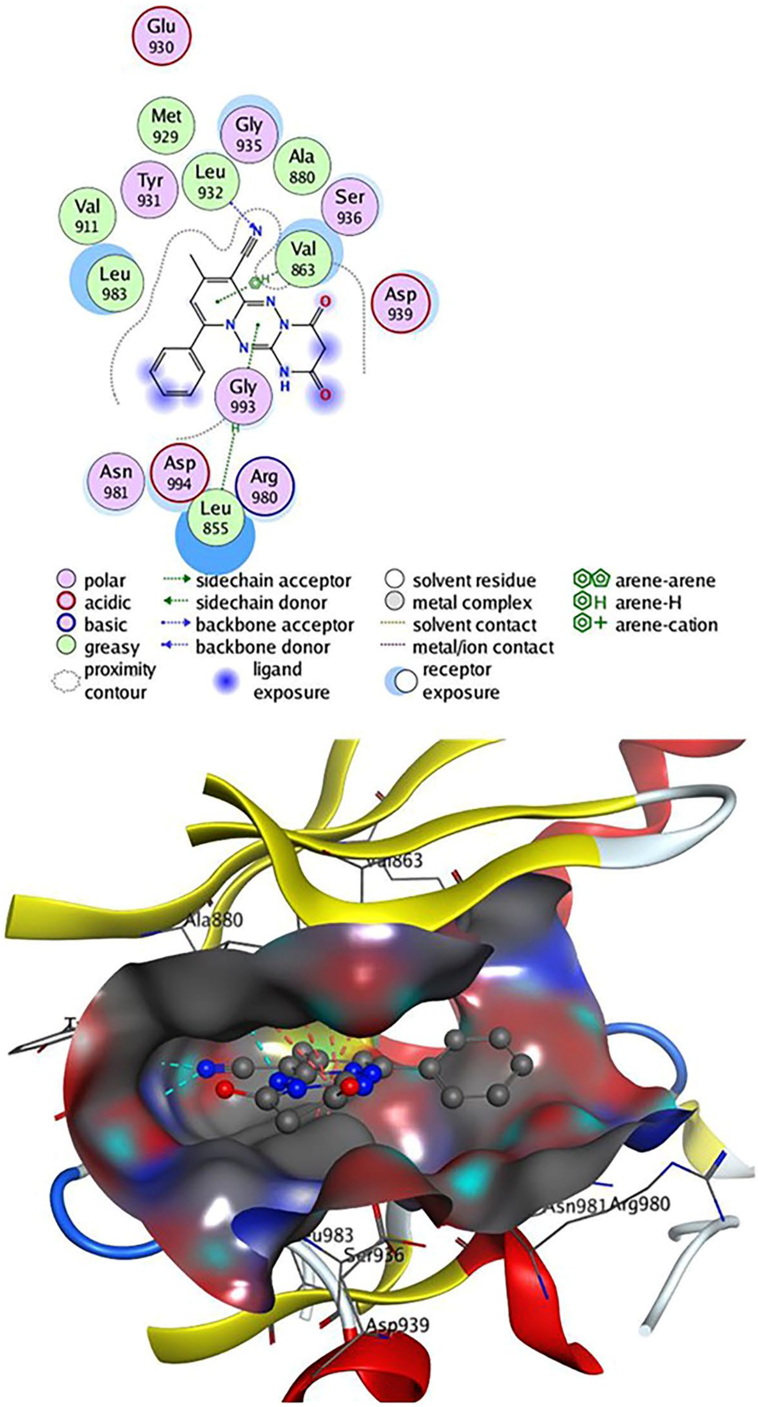

Figure 8. 2D& 3D interaction of **8** in the active site of Janus kinase **Jak2** (PDB ID: **4P7E**). Hydrogen bonds are displayed in cyan & H-pi-bonds are in dark pink.

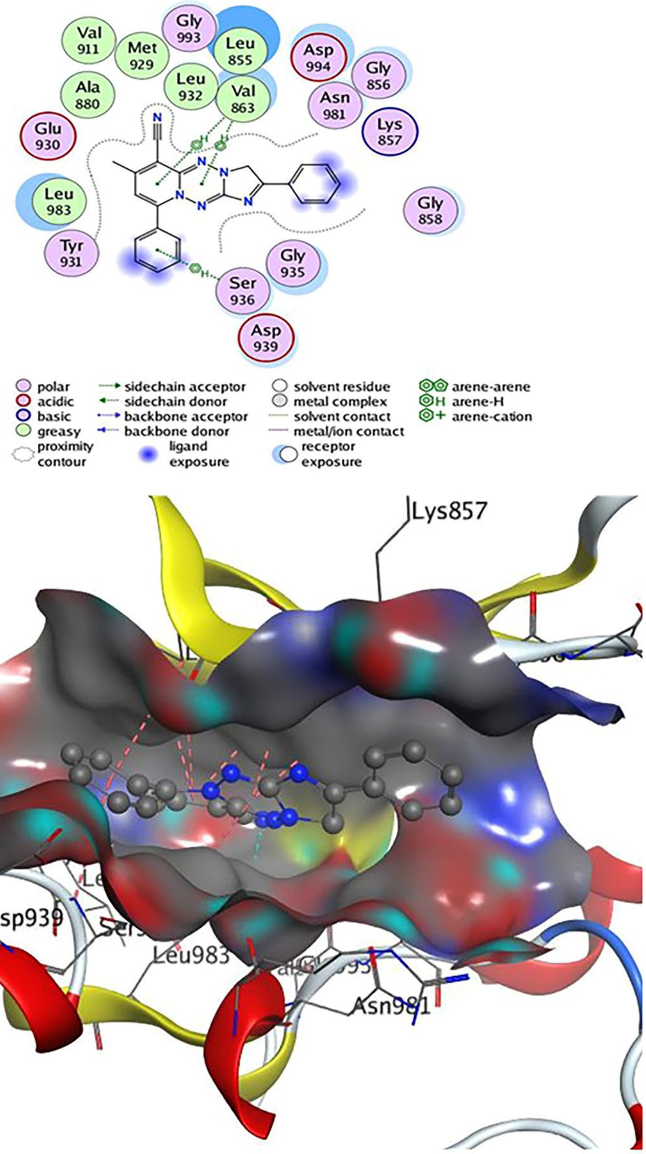

Figure 9. 2D& 3D interaction of **9** in the active site of Janus kinase **Jak2** (PDB ID: **4P7E**). Hydrogen bonds are displayed in cyan & H-pi-bonds are in dark pink.

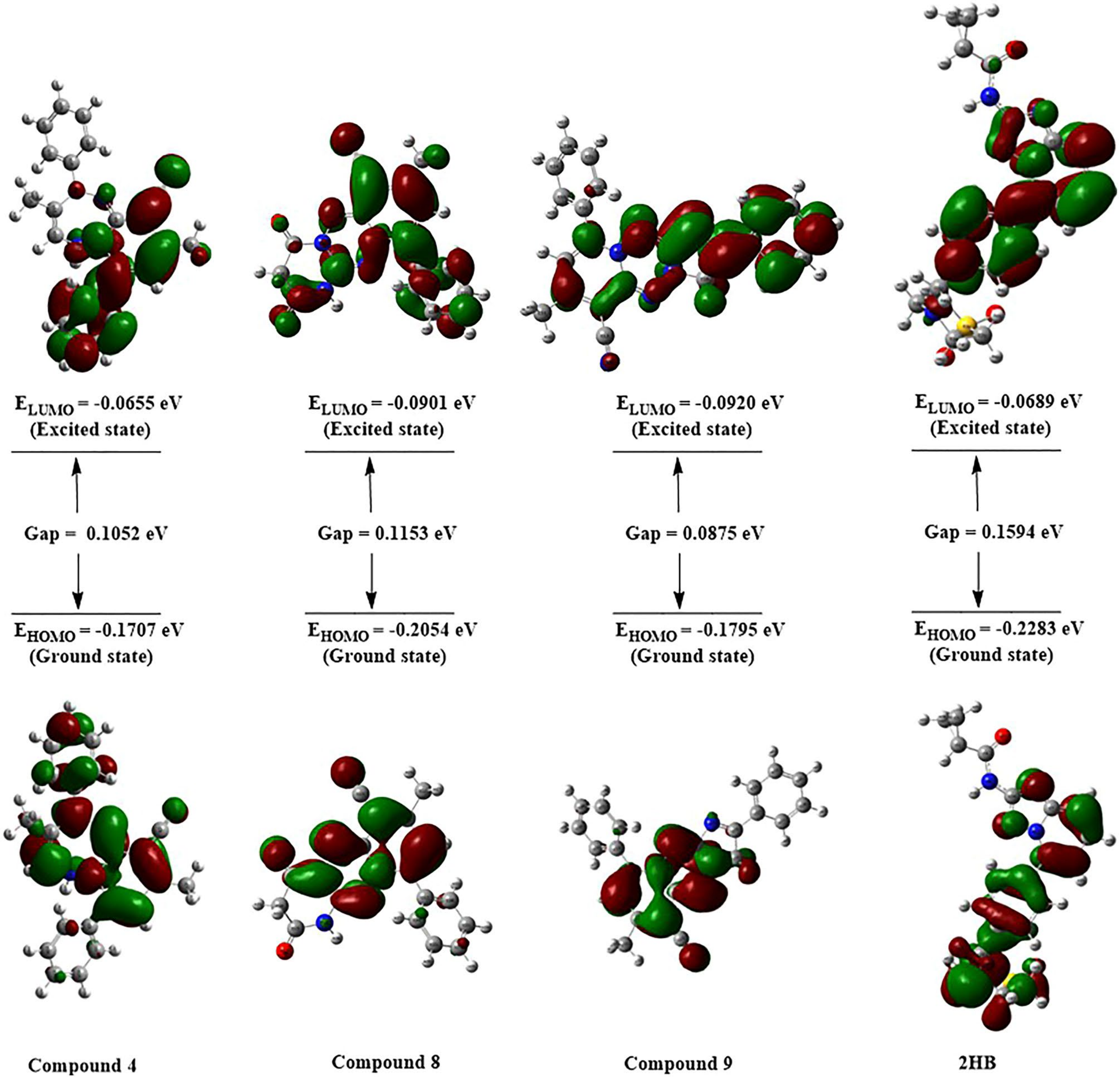

Figure 10. Molecular orbital distribution plots of HOMO and LUMO for compounds **4**, **8**, **9,** and **2HB.**

Comp No.	Dipole moment, μ (Debye)	E_{HOMO} (eV)	E_{LUMO} (eV)	(HOMO–LUMO) gaps (eV)
4	8.2089	−0.1707	−0.0655	0.1052
8	9.7371	−0.2054	−0.0901	0.1153
9	5.0329	−0.1795	−0.0920	0.0875
2HB	7.2947	−0.2283	−0.0689	0.1594

Table 3. DFT parameters calculated for the synthesized compounds (**4, 8, 9**) & **2HB**. *DFT* density functional theory, *HOMO* highest occupied molecular orbital, *LUMO* lowest unoccupied molecular orbital.

Comp. No.	Chemical structure	Optimized structure
4	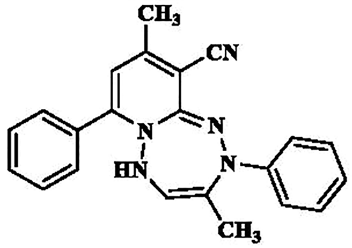	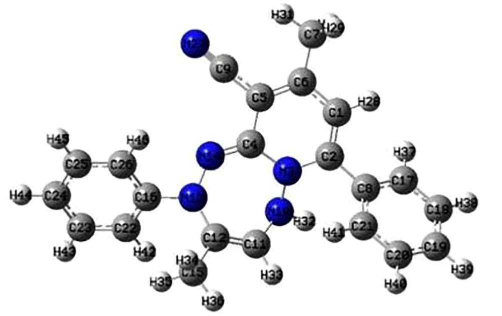
8	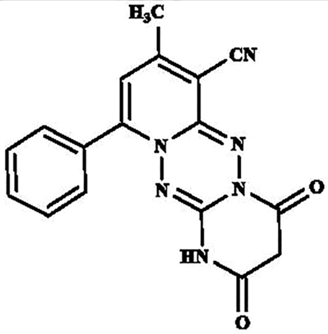	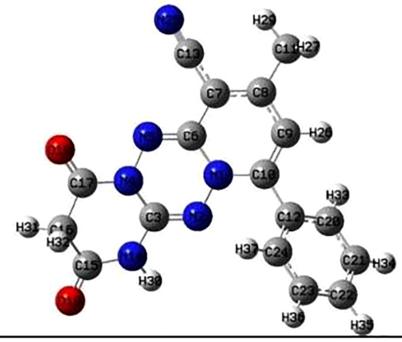
9	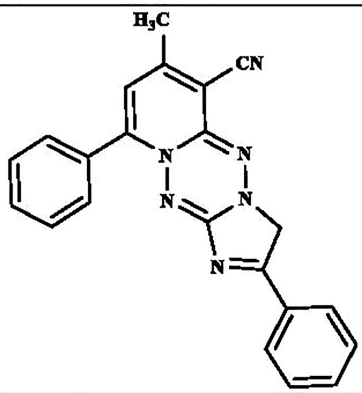	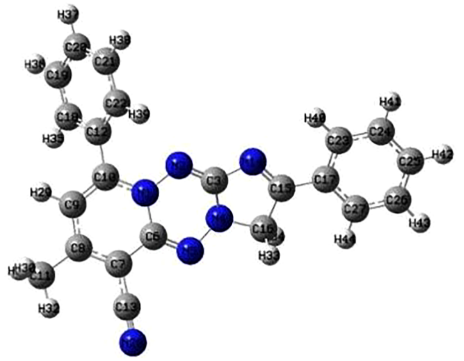
2HB	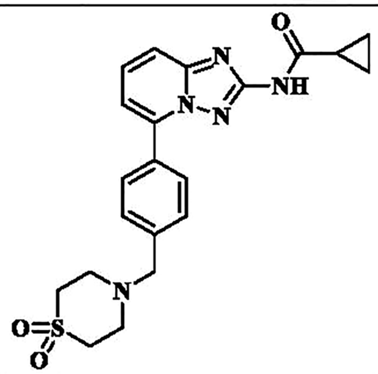	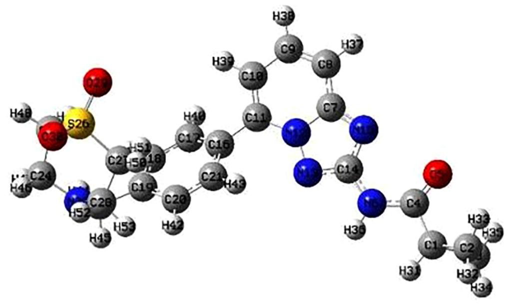

Figure 11. Chemical and optimized structure of compounds (**4**, **8**, **9**) and **2HB**. Optimized with DFT-B3LYP/6-31G.

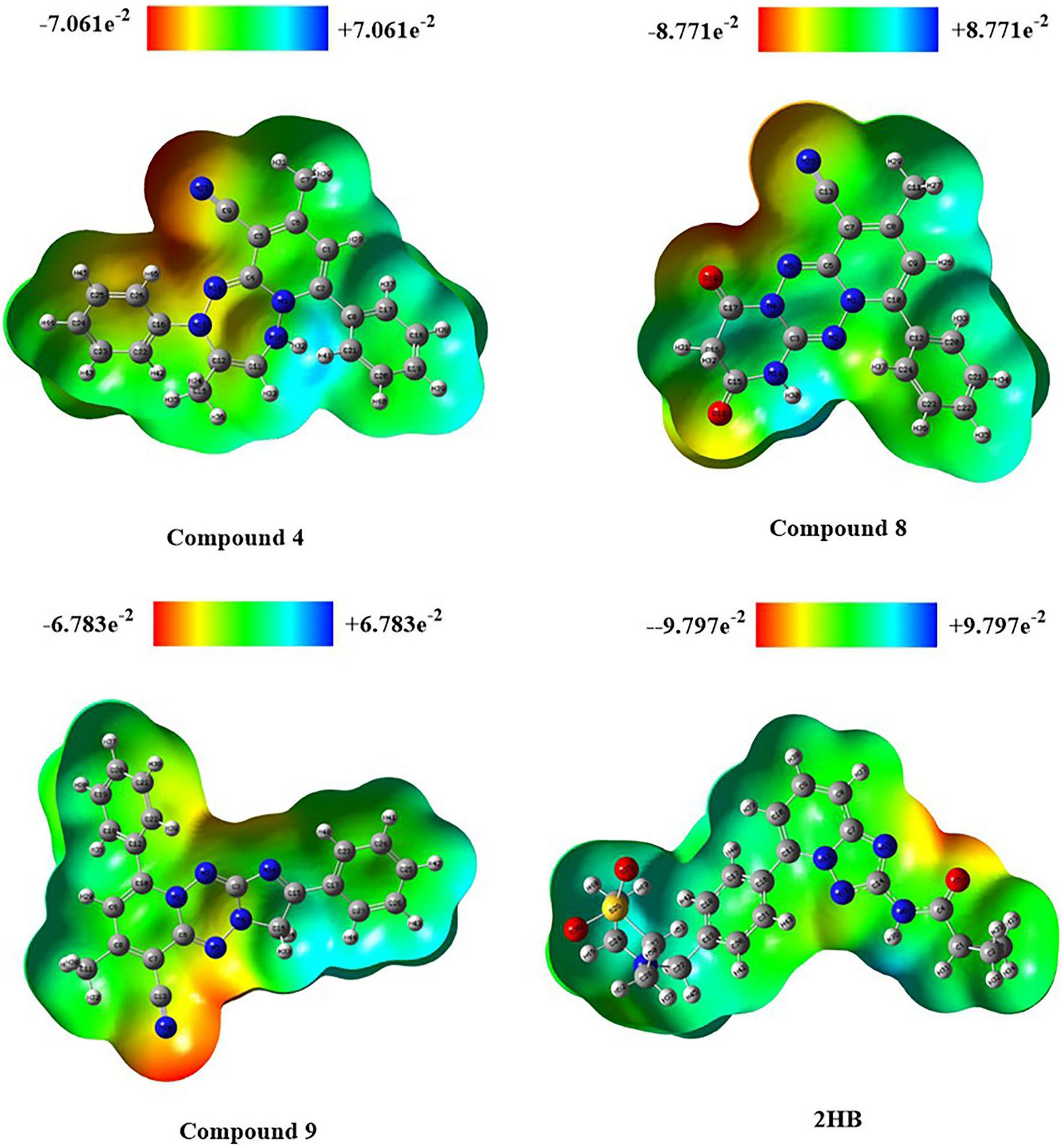

Figure 12. MEP map of compounds (**4**, **8**, **9**) and **2HB**.

Molecule	[a]MW ≤ 500	[b]Log $P_{o/w}$ ≤ 5	[c]TPSA $Å^2$ ≤ 140	[d]NRB ≤ 10	[e]Log S	[f]HBA ≤ 10	[g]HBD ≤ 5	Lipinski violations
(**4**)	353.42	4.73	61.81	2	− 5.9**	2	1	0
(**8**)	332.32	1.35	105.08	1	− 3.45*	5	1	0
(**9**)	364.4	3.69	71.27	2	− 5.17**	4	0	0
(**2HB**)	425.5	2.27	105.05	6	− 3.31*	6	1	0

Table 4. In silico physicochemical properties and drug-likeness of compounds **4, 8,** and **9,** as well as the reference **2HB.** [a]MW, molecular weight. [b]Log $P_{o/w}$, partition coefficient octanol/water. [c]TPSA, topological polar surface area. [d]NRB, number of rotatable bonds. [e]Log S, Aqueous solubility (*soluble, **moderately soluble). [f]HBA, number of H-bond acceptors. [g]HBD, number of H-bond donors.

Cpd. No.	BBB permeant	GI absorption	Pgp substrate	Cytochrome P450 (CYP inhibitor)				
				CYP1A2 inhibitor	CYP2C19 inhibitor	CYP2C9 inhibitor	CYP2D6 inhibitor	CYP3A4 inhibitor
(**4**)	Yes	High	No	Yes	Yes	Yes	Yes	No
(**8**)	No	High	No	No	No	No	No	No
(**9**)	Yes	High	No	Yes	Yes	Yes	No	No
(**2HB**)	No	High	Yes	No	No	Yes	No	Yes

Table 5. In silico pharmacokinetic study of compounds **4, 8,** and **9** as well as the reference **2HB.**

Data availability
The datasets generated and analyzed during the current study are available at https://www.scidb.cn/anonymous/aUFSYlF6.

Received: 26 December 2022; Accepted: 27 March 2023
Published online: 05 April 2023

References
1. Abdel-Raheem, S. *et al.* A concise review on some synthetic routes and applications of pyridine scaffold compounds. *Curr. Chem. Lett.* **10**(4), 337–362 (2021).
2. Kotb, E. R., Abbas, H. A. S., Flefel, E. M., Sayed, H. H. & Abdelwahed, N. A. Utility of hantzsch ester in synthesis of some 3, 5-bis-dihydropyridine derivatives and studying their biological evaluation. *J. Heterocycl. Chem.* **52**(5), 1531–1539 (2015).
3. Flefel, E., Abbas, H. A., Abdel Mageid, R. & Zaghary, W. Synthesis and cytotoxic effect of some novel 1, 2-dihydropyridin-3-carbonitrile and nicotinonitrile derivatives. *Molecules* **21**(1), 30 (2015).
4. El-Sayed, A. A. *et al.* Anti proliferative activity for newly heterofunctionalized pyridine analogues. *PONTE Int. J. Sci. Res.* **72**(7), 106–118 (2016).
5. Sayed, H. H., Morsy, E. M. & Flefel, E. M. Synthesis and reactions of some novel nicotinonitrile, thiazolotriazole, and imidazolotriazole derivatives for antioxidant evaluation. *Synthetic Commun.* **40**(9), 1360–1370 (2010).
6. Sayed, H. H., Flefel, E. M., Abd El-Fatah, A. M. & El-Sofany, W. I. Focus on the synthesis and reactions of some new pyridine carbonitrile derivatives as antimicrobial and antioxidant agents. *Egypt J. Chem* **53**, 17–35 (2010).
7. Abdelhameed, R. M., El-Sayed, H. A., El-Shahat, M., El-Sayed, A. A. & Darwesh, O. M. Novel triazolothiadiazole and triazolothiadiazine derivatives containing pyridine moiety: Design, synthesis, bactericidal and fungicidal activities. *Curr. Bioact. Compd.* **14**(2), 169–179 (2018).
8. Rashad, A. E. *et al.* Synthesis and anti-avian influenza virus (H5N1) evaluation of some novel nicotinonitriles and their N-acylic nucleosides. *J. Heterocyclic Chem.* **49**(5), 1130 (2012).
9. Serrar, H. *et al.* Synthesis and evaluation of novel pyrido [1, 2-b][1, 2, 4] triazine-2, 6-dione and pyrido [1, 2-b][1, 2, 4] triazepine-2, 7-dione derivatives as antioxidant agents. *Lett. Org. Chem.* **14**(4), 267–277 (2017).
10. Elattar, K. M., Abozeid, M. A., Mousa, I. A. & El-Mekabaty, A. Advances in 1, 2, 4-triazepines chemistry. *RSC Adv.* **5**(129), 106710–106753 (2015).
11. Ali, T. E. S. & Ibrahim, M. A. Synthesis and antimicrobial activity of chromone-linked 2-pyridone fused with 1, 2, 4-triazoles, 1, 2, 4-triazines and 1, 2, 4-triazepines ring systems. *J. Braz. Chem. Soc.* **21**, 1007–1016 (2010).
12. Pandey, S. K., Singh, A. & Singh, A. Antimicrobial studies of some novel quinazolinones fused with [1, 2, 4]-triazole,[1, 2, 4]-triazine and [1, 2, 4, 5]-tetrazine rings. *Eur. J. Med. Chem.* **44**(3), 1188–1197 (2009).
13. Xia, J. *et al.* ZGDHu-1 induces G2/M phase arrest and apoptosis in Kasumi-1 cells. *Mol. Med. Rep.* **11**(5), 3398–3404 (2015).
14. Chen, S. F. *et al.* N, N′-di-(m-methylphenyi)-3, 6-dimethyl-1, 4-dihydro-1, 2, 4, 5-tetrazine-1, 4-dicarboamide (ZGDHu-1) suppresses the proliferation of PANC-1 pancreatic cancer cells via apoptosis and G2/M cell cycle arrest. *Oncol. Rep.* **33**(4), 1915–1921 (2015).
15. Xu, F. *et al.* Synthesis, antitumor evaluation and molecular docking studies of [1, 2, 4] triazolo [4, 3-b][1, 2, 4, 5] tetrazine derivatives. *Bioorg. Med. Chem. Lett.* **26**(13), 3042–3047 (2016).
16. Kamata, M. *et al.* Symmetrical approach of spiro-pyrazolidinediones as acetyl-CoA carboxylase inhibitors. *Bioorg. Med. Chem. Lett.* **22**(14), 4769–4772 (2012).
17. Darehkordi, A., Khorasani, F. N., Mohammadi, M. & Kazemi, E. I2/KI-Catalyzed synthesis of 5-trifluoromethylated 1, 2, 4, 6-tetrazepine-3-thiones by annulation of trifluoroacetimidoyl chlorides and thiosemicarbazones. *Monatshefte für Chemie-Chemical Monthly* **151**(12), 1835–1839 (2020).
18. Clarke, P. A., Santos, S. & Martin, W. H. C. Combining pot, atom and step economy (PASE) in organic synthesis Synthesis of tetrahydropyran-4-ones. *Green Chem.* **9**(5), 438. https://doi.org/10.1039/b700923b (2007).
19. Elgemeie, G. H., & Hussain, B. W. Reactions of acylthiosemicarbazides with β-diketones: Novel synthesis of N-(1-pyridyl) thiourea derivatives. *J. Chem. Res. Synopses (Print)*issn 0308–2342. (3), 87 (1993).
20. Monks, A. *et al.* Feasibility of a high-flux anticancer drug screen using a diverse panel of cultured human tumor cell lines. *JNCI J. Natl. Cancer Inst.* **83**(11), 757–766. https://doi.org/10.1093/jnci/83.11.757 (1991).
21. Enviroment, M. O. (2015). Chemical Computing Group, Inc; Montreal, Quebec, Canada.
22. Hassan, A. Y., Saleh, N. M., Kadh, M. S. & Abou-Amra, E. S. New fused pyrazolopyrimidine derivatives; heterocyclic styling, synthesis, molecular docking and anticancer evaluation. *J. Heterocycl. Chem.* **57**(7), 2704–2721 (2020).
23. Gaussian, R. A. *et al.* (Gaussian, Inc, Wallingford CT, 2009). https://gaussian.com/g09citation/ [Accessed 14 April 2022].
24. Becke, A. D. Density-functional exchange-energy approximation with correct asymptotic behavior. *Phys. Rev. A* **38**(6), 3098–3100. https://doi.org/10.1103/PhysRevA.38.3098 (1988).
25. Lee, C., Yang, W. & Parr, R. G. Development of the Colle-Salvetti correlation-energy formula into a functional of the electron density. *Phys. Rev. B* **37**(2), 785–789. https://doi.org/10.1103/PhysRevB.37.785 (1988).
26. Saravanan, S. & Balachandran, V. Quantum chemical studies, natural bond orbital analysis and thermodynamic function of 2,5-dichlorophenylisocyanate. *Spectrochim. Acta Part A Mol. Biomol. Spectrosc.* **120**, 351–364. https://doi.org/10.1016/j.saa.2013.10.042 (2014).
27. Politzer, P. & Murray, J. S. Molecular electrostatic potentials and chemical reactivity. *Rev. Comput. Chem.* **2**, 273–312 (1991).
28. Daina, A. & Zoete, V. A boiled-egg to predict gastrointestinal absorption and brain penetration of small molecules. *ChemMedChem* **11**, 1117–1121 (2016).

Acknowledgements
The authors would like to express their profound thanks to the National Institutes of Health (NIH), Bethesda, MD, USA, for the anticancer screening trials provided in this paper.

Author contributions
All authors were involved in the synthesis, structure elucidation, and writing-original draft preparation.

Funding
Open access funding provided by The Science, Technology & Innovation Funding Authority (STDF) in cooperation with The Egyptian Knowledge Bank (EKB). This research did not receive any specific grant from funding agencies.

Competing interests
The authors declare no competing interests.

Additional information
Supplementary Information The online version contains supplementary material available at https://doi.org/10.1038/s41598-023-32421-x.

Correspondence and requests for materials should be addressed to E.S.A.-A.

Reprints and permissions information is available at www.nature.com/reprints.

Publisher's note Springer Nature remains neutral with regard to jurisdictional claims in published maps and institutional affiliations.